NASA
Technical
Paper
2100

January 1983

Pressures, Forces and Moments, and Shock Shapes for a Geometrically Matched Sphere-Cone and Hyperboloid at Mach 20.3 in Helium

Robert L. Calloway

NASA

NASA
Technical
Paper
2100

1983

Pressures, Forces and Moments, and Shock Shapes for a Geometrically Matched Sphere-Cone and Hyperboloid at Mach 20.3 in Helium

Robert L. Calloway
Langley Research Center
Hampton, Virginia

National Aeronautics
and Space Administration

Scientific and Technical
Information Branch

INTRODUCTION

For ballistic entry, the sphere-cone shape has been a primary subject of study and design since the idea of returning a vehicle through the Earth's atmosphere was first conceived. Results from experimental studies conducted on sphere-cones at supersonic and hypersonic Mach numbers are extensive. Most of the early work was conducted on cones with small half-angles (less than 40°) because they were candidates for ballistic reentry into our own atmosphere. References 1 and 2 provide summary tables and a compilation, respectively, of the major body of data on cones up through the mid-1960's. Particular examples of some of the early experimental work are given in references 3 to 13. In later work (refs. 14 to 22), cones with larger half-angles were studied with increasing interest as candidates for planetary entry probe configurations; these studies used several test gases such as helium, carbon dioxide, and tetrafluoromethane (refs. 23 to 28). Moreover, the sphere-cone has been used as the forebody shape of probes for the Viking Project (Mars) and Pioneer Venus, and it is planned for use on Project Galileo (Jupiter).

Because of the severe heating environments and the associated complex flow fields during planetary entry, final aerothermodynamic design for probes must be determined using computational methods, with experimental results used to validate these methods and to provide a data base for inputs to empirical techniques or correlation procedures (ref. 29). As computational techniques have been developed for the design of sphere-cone entry probes, work on so-called "analytical shapes" such as the hyperboloid, paraboloid, and ellipsoid has also flourished. The analytical shapes, with their continuous surface curvatures and smoother variations of flow properties, are ideal for study using computational techniques. Although the discontinuity in surface curvature at the junction point on the sphere-cone has been managed by theoreticians, it is still a problem and one that increases as more complex flow models are developed. Certainly, analytical shapes are more amenable for use with complex theoretical techniques. Since hyperboloid shapes can be adjusted to match sphere-cone shapes almost identically, the hyperboloid could possibly replace the sphere-cone with no loss in performance but a substantial gain in the ability to analyze the flow field.

The present investigation examines the measured and predicted pressure distributions, forces and moments, and shock shapes for a geometrically matched sphere-cone and hyperboloid. A sphere-cone with a cone half-angle of 45° and a nose-to-base radius ratio of 0.50 was chosen, since this particular shape was used for the Venusian probes and is planned for use on the Jovian probe. The nose bluntness and the asymptotic angle of a hyperboloid were adjusted to match the shape of the sphere-cone as closely as possible with identical lengths and base diameters. The matching hyperboloid has a nose radius of 0.5276 in. and an asymptotic angle of 39.9871°. Two sets of models (one for pressure tests and one for force and moment tests) were constructed for each shape. All tests were conducted in the 22-inch aerodynamics leg of the Langley Hypersonic Helium Tunnel Facility at a free-stream Mach number of 20.3 and a free-stream unit Reynolds number of 6.83×10^6 per foot. Predictions from a theoretical method by Kumar and Graves (ref. 30) were used for comparisons with the measured results.

SYMBOLS

A	model base area, in^2
A_b	area over which base pressure is assumed to act, in^2
a	distance from vertex to center of hyperbola, in.
b	distance from vertex to asymptotes (perpendicular to transverse axis), in.
C_A	axial-force coefficient, $\frac{\text{Axial force}}{qA}$
C_{A_B}	base-pressure correction coefficient (eq. (6))
C_{A_C}	axial-force coefficient corrected for base pressure (eq. (6))
C_D	drag coefficient, $\frac{\text{Drag force}}{qA}$
C_L	lift coefficient, $\frac{\text{Lift force}}{qA}$
C_m	pitching-moment coefficient, $\frac{\text{Pitching moment}}{qAd}$
C_N	normal-force coefficient, $\frac{\text{Normal force}}{qA}$
d	model base diameter, in.
L/D	lift-drag ratio
M	Mach number
M_∞	free-stream Mach number
p	pressure, psia
p_b	base pressure, psia
p_o	pressure value at $s = 0$, psia
p_t	stagnation pressure, psia
p_∞	free-stream pressure, psia
q	free-stream dynamic pressure, psia
$R_{\infty,d}$	free-stream Reynolds number based on d
r_b	model base radius, in.
r_n	model nose radius, in.

r_n/r_b	nose bluntness ratio
s	coordinate measured along body surface (fig. 2(a)), in.
s_t	total distance from nose to corner (along body surface), in.
T	temperature, °R
T_t	stagnation temperature, °R
V_∞	free-stream velocity, ft/sec
x,r	cylindrical coordinates (fig. 2(a))
$\bar{x},\bar{r}$	cylindrical coordinates nondimensionalized by r_n
α	angle of attack, deg
θ	cone half-angle or asymptotic angle, deg
μ	dynamic viscosity, slugs/ft-sec
ϕ	roll angle, deg

EXPERIMENTAL APPARATUS AND TEST PROCEDURES

Facility and Test Conditions

The experimental results presented herein were obtained in the 22-inch aerodynamics leg of the Langley Hypersonic Helium Tunnel Facility, which is a closed-cycle, blowdown facility. The facility has a contoured axisymmetric nozzle which expands the flow into a windowed test section (fig. 1) having a nominal cross-section diameter of 22 in. An electron-beam device is mounted atop the test section to provide flow-visualization capability. Calibration surveys (ref. 31) indicate a range of average test-core Mach numbers from 17.2 to 22.2 at stagnation presssures of 200 psia to 3000 psia, respectively. The facility can be operated at stagnation temperatures from ambient to 960°R. The average duration of a test run is 30 sec. The helium is then collected, purified, and stored in high-pressure tanks for subsequent tests. Operation of this facility and details of the flow characteristics are presented in reference 31. All present tests were conducted at the following nominal flow conditions:

$M_\infty = 20.3$

$p_t = 1015$ psia

$T_t = 520°R$

$R_{\infty,d} = 1.71 \times 10^6$

Models

The hyperboloid shape was matched to the sphere-cone shape ($\theta = 45°$, $r_n/r_b = 0.50$) using equations based on the coordinates in figure 2(a). The two shapes were constrained for identical lengths and base diameters and were to match coordinates as closely as possible. Taking just the $x > 0$ portion of a hyperbola with the vertex at (0,0) and the center (asymptote junction) at (-a,0), the general equation is as follows:

$$\frac{(x + a)^2}{a^2} - \frac{r^2}{b^2} = 1 \tag{1}$$

Equation (1) can be simplified as follows:

$$r^2 = 2\,\frac{b^2}{a}\,x + \frac{b^2}{a^2}\,x^2 \tag{2}$$

or in dimensional form,

$$r^2 = 2r_n x + x^2 \tan^2\theta \tag{3}$$

The nondimensional form is obtained by setting $\bar{r} = r/r_n$ and $\bar{x} = x/r_n$:

$$\bar{r}^2 = 2\bar{x} + \bar{x}^2 \tan^2\theta \tag{4}$$

Using the dimensional form of the equation for the hyperbola, r_n and θ values were iterated until the following were obtained:

$$\frac{b^2}{a} = r_n = 0.5276 \text{ in.} \qquad \frac{b^2}{a^2} = \tan^2\theta = 0.7034$$

where $\theta = 39.9871°$.

This equation in actual coordinates (for x and r in inches)

$$r^2 = 1.0552x + 0.7034x^2 \tag{5}$$

produced the match as shown in figure 2(b).

A pressure model and a force-test model with base diameters of 3.00 in. were fabricated for both the sphere-cone and hyperboloid shapes. (See fig. 3.) Each pressure model was designed with 16 orifices (all in the same plane) which were spaced at s/s_t locations from 0 to 0.956 on the sphere-cone and 0 to 0.939 on the hyperboloid. A sketch of each pressure model and the orifice locations are presented in figure 4. The pressure models were machined from stainless steel, and the orifice-location holes were drilled with a jigbore. Stainless steel tubing with 0.020 in. inside diameter was then cemented into the orifice location.

Force-test models (used also for shock-shape tests) were also machined from stainless steel. (See fig. 5.) The tapered cylindrical section extending behind the model forebody was designed to house the strain-gage balance and to have no interference effects on the measured aerodynamic forces and moments.

Test Methods

The pressure measurements were conducted with the pressure models attached to a hollow sting which housed the pressure tubing. The tubing diameter was increased as much as possible to reduce settling-out times, and the tubes were connected to a standard manifold system to allow each orifice and its associated plumbing to be properly tested for leaks. Calibrated, capacitance-type pressure transducers were used in conjunction with signal conditioning units to record the data onto magnetic tape. Reference pressure runs were conducted daily using a registered "standard" device to help ensure data accuracy. For each model, the angle of attack was set using a cathetometer, and the roll angle was set using an attached fixture and an inclinometer. Pressure data were recorded for $\alpha = 0°$, 5°, 10°, 15°, and 18° and $\phi = 0°$, 22.5°, 45°, 67.5°, 90°, 112.5°, 135°, 157.5°, and 180°. Pressure data on all 16 orifices were recorded for 1 angle of attack and 1 roll angle for each run. Run times varied from about 20 sec to 35 sec depending upon angle of attack. Data were recorded continuously over the last portion of the runs, and the time histories were analyzed to confirm steady-state values. Before changing the model roll-angle setting, data were obtained for all angles of attack. Model roll angle was defined as 0° when all orifices were in the vertical plane with orifice number 15 at the top. By rolling the model 180° in 22.5° increments, pressures were determined for all 16 s/s_t locations for all 9 meridional planes by using model symmetry.

Force and moment tests were conducted with the models mounted on a sting-supported, six-component strain-gage balance. The straight sting was attached to the angle-of-attack mechanism, and data were obtained for 2.5° increments from −5° to 17.5°. The angle of attack was set optically by using a point light source adjacent to the test section and a small lens-prism mounted on the rearward extension of the model. The image of the source was reflected by the prism and focused by the lens onto photoelectric cells aligned at calibrated intervals. As reflected and focused light swept past each cell (the model is swept continuously for force-test runs), an electrical relay was energized and caused a high-speed digital recorder to sample and record the outputs of the strain-gage balance onto magnetic tape. The data were then reduced using a standard force-test program. The accuracy of the angle of attack is estimated to be ±0.1°. Model base pressures were measured at one location (see fig. 6), and the axial-force coefficient C_A was corrected using the following equation:

$$C_{A_C} = C_A - C_{A_B} \tag{6}$$

where

$$C_{A_B} = \frac{(p_\infty - p_b)}{q} \frac{A_b}{A}$$

The value of A_b was determined by subtracting the cross-sectional area (in the base plane) of the tapered cylindrical section from the total base area of the force-test models.

The reference area for the models was the base area A, and the reference length was the base diameter d. The pitching-moment data were reduced about the nose of each model. The total estimated uncertainties in the measured static aerodynamic coefficients based on ±0.5 percent of the balance design loads and the uncertainties in tunnel facility flow conditions are as follows:

ΔC_N .... ±0.003
ΔC_A .... ±0.007
ΔC_m .... ±0.001

Quantitative shock-shape measurements in the plane of symmetry for $\alpha = 0°$, 5°, 10°, 15°, and 18° were obtained by using the electron-beam fluorescence technique described in reference 32. Photographs of the models in the illuminated flow field were taken with a camera positioned with its optical axis normal to the plane of symmetry. (See fig. 6.) The angle of attack was set with a cathetometer before each run. Calculations to estimate the error introduced by using conical field-of-view photographs for measuring shock shapes as opposed to a parallel-light, schlieren-type system showed the error to be less than 0.3 percent. The shock-shape values were digitized from photographs similar to the one shown in figure 7 for the hyperboloid at $\alpha = 15°$.

All measured pressure and shock-shape values on the sphere-cone and hyperboloid are presented in tables I, II, III, and IV.

PREDICTION METHOD

The prediction method of Kumar and Graves (ref. 30) was used exclusively in this investigation, since it is one of the few methods available which consider both viscous flow and bodies at angles of attack. Also, it is shown in reference 28 that results from this prediction method show generally excellent agreement with measured results on sphere-cones. This method calculates the laminar and turbulent hypersonic flows in the plane of symmetry about blunt axisymmetric bodies which have outflow boundaries that are predominately supersonic; thus, the angle of attack for which a solution will be valid is limited, since a sonic corner condition may be approached in the windward symmetry plane as the angle of attack increases. In addition, the form of the assumed meridional pressure distribution used in the solution becomes less accurate as the angle of attack increases and thus further restricts the solution to small angles of attack.

The code (described in ref. 33) is written in STAR FORTRAN language for the Control Data CYBER 203 computer (upgraded from Control Data STAR-100). Timedependent, viscous-shock-layer-type equations are used to describe the flow field, and these equations are solved by an explicit, two-step, time-asymptotic finite-difference method. Although the code was originally written for air acting as a perfect gas and used Sutherland's viscosity law, it was modified for this investigation to consider helium as a perfect gas and to use the following modified form of the Sutherland viscosity law (ref. 34):

$$\mu = 7.173 \frac{T^{1.647}}{T + 1.5} \times 10^{-9} \tag{7}$$

where μ is in slugs/ft-sec and T is in °R. The flow was assumed to be laminar for all cases.

RESULTS AND DISCUSSION

Pressure Distributions

Measured pressures, normalized by the value measured at orifice number 1 (where $s/s_t = 0$), are presented versus s/s_t for the sphere-cone and hyperboloid in figure 8 for all values of α and ϕ. In general, the measured sphere-cone pressures are lower than the measured hyperboloid pressures in the overexpansion region but are higher than the hyperboloid pressures along the skirt region. For $\alpha < 15°$, the sphere-cone also exhibits a much larger pressure gradient near $s/s_t = 1$ as the surface pressure expands rapidly to reach sonic conditions at the corner. For $\alpha = 15°$ and $18°$ and $\phi > 135°$ (figs. 8(g), (h), and (i)), the measured pressures for both shapes are very similar, probably because the local flow is subsonic. For all values of α and ϕ, the pressure distributions on the hyperboloid are significantly smoother than those on the sphere-cone.

Comparisons between measured and predicted pressure distributions on the sphere-cone are presented in figure 9, with the pressure values nondimensionalized by twice the free-stream dynamic pressure (2q). The disagreement between measured and predicted values near $s/s_t = 0$ is due to a higher-than-the-average Mach number on the tunnel centerline. In reference 31, tunnel calibrations at the same flow conditions and location show the centerline Mach number to be about 0.5 higher than the average test-core Mach number of 20.3, but at locations ±1/2 in. from the centerline, the Mach number deviation is only ±0.1. If the measured pressures in this region of disagreement were divided by the free-stream dynamic pressure based on a Mach number of 20.8, the agreement would be excellent. Thus, in the discussion of the pressure-distribution comparisons (figs. 9 and 10) which follow, the disagreement between measured and predicted values near $s/s_t = 0$ will be ignored.

Measured and predicted pressure distributions on the sphere-cone for $\alpha = 0°$ (fig. 9(a)) show excellent agreement except at the aft end (corner) of the body, where the prediction method is not designed to account for the proper corner solution ($M = 1$). The experimental pressure data indicate subsonic flow over the surface and approach the sonic pressure value at the corner. These results complement those of reference 28 in which predicted sonic lines in the shock layer show a subsonic nose region and a mixed (subsonic and supersonic) region on the skirt with a Mach 1 condition at the corner and predominately supersonic outflow. For $\alpha = 5°$ (fig. 9(b)), the predicted values are in reasonably good agreement with the measured values except near the end point ($s/s_t = 1$). The first clear sign of a breakdown in the prediction technique for sphere-cone pressures is observed for $\alpha = 10°$ (fig. 9(c)). On both the leeward and windward sides the predicted pressures are higher than the measured values and diverge significantly away from the measured values toward the end of the body. This set of results is considered to be outside the range of applicability of the prediction method, probably because of the large crossflow velocity gradients and a subsonic outflow region on the windward side for this angle of attack.

Comparisons between measured and predicted pressure distributions on the hyperboloid are presented in figure 10. For $\alpha = 0°$ (fig. 10(a)), the agreement between measured and predicted values is excellent, even near the corner. For $\alpha = 5°$ and 10° (figs. 10(b) and (c)), there is excellent agreement between measured and predicted pressures except on the windward side near the sonic corner for $\alpha = 10°$. For $\alpha = 15°$ (fig. 10(d)), the divergent character of the predicted pressures is similar to that obtained for the sphere-cone at $\alpha = 10°$. Therefore, the prediction method is considered invalid at this angle of attack.

Static Aerodynamic Coefficients

Measured and predicted results are used to compare the static aerodynamic coefficients for the sphere-cone and hyperboloid (fig. 11). The static aerodynamic characteristics are essentially the same for the two shapes except for C_{A_C} and C_D. Note that the longitudinal stability (fig. 11(b)) and the lift-drag ratio (fig. 11(c)) for the sphere-cone and hyperboloid are (within measuring accuracy) essentially identical. However, for small angles of attack ($\alpha < 10°$), the measured C_{A_C} and C_D for the sphere-cone are approximately 4 percent higher than for the hyperboloid. This was expected from observation of the pressure distributions, which show that the measured pressures on the sphere-cone are greater in the skirt region - where the surface area is larger. Also included in figures 11(a) and (b) are values which were obtained by integrating both the measured and predicted pressures. Comparisons between force-test results and the integrated measured pressures are good, with a maximum difference of 2 percent for C_{A_C} at $\alpha = 0°$ (fig. 11(a)). Aerodynamic coefficients which were obtained by integrating the predicted pressures also show good agreement. As α increases, the increasing differences in measured and predicted C_{A_C} (fig. 11(a)) are due to approaching the limit of the range of applicability of the prediction method.

Figure 11(b), with an expanded scale, shows that the C_{A_B} values are relatively small compared with total measuring accuracies.

Shock Shapes

Measured shock shapes are presented in figure 12 for the sphere-cone and hyperboloid for $\alpha = 0°$, 5°, 10°, 15°, and 18°. For all five values of α, the shock shapes are essentially identical in the nose region. For $\alpha = 0°$ (fig. 12(a)), there is an inflection point in the shock shape for the sphere-cone caused by the overexpansion-recompression region. The hyperboloid shock shape is smoother and has a slightly greater standoff distance in the skirt region compared with the sphere-cone. The latter observation is as expected, since the measured surface pressure on the hyperboloid is less than that measured on the sphere-cone. (See fig. 8 for $\alpha = 0°$.) Higher pressures mean higher densities in the shock layer; thus, less distance (volume) is required for an equivalent amount of mass in that region.

For $\alpha = 5°$, $10°$, and $15°$ (figs. 12(b), (c), and (d)), the comparisons are similar. Within the accuracy of the measurements, the shock shapes for both bodies are about the same on the windward side; however, on the leeward side the sphere-cone shock standoff distance is less than that for the hyperboloid. For $\alpha = 18°$ (fig. 12(e)), there appear to be exactly opposite trends on the windward and leeward sides. On the windward side the sphere-cone shock standoff distance is less than that for the hyperboloid; however, on the leeward side the sphere-cone shock standoff distance is greater than that for the hyperboloid.

The predicted shock shapes for both the sphere-cone and hyperboloid are presented in figure 13 for $\alpha = 0°$ and $5°$. No comparisons are presented for $\alpha > 5°$ because one or both of the solutions break down for these higher angles of attack. The comparisons for $\alpha = 0°$ and $5°$ (figs. 13(a) and (b)) are similar; the greater bluntness of the sphere-cone nose for these bodies causes the shock to stand off slightly more in that region. Farther downstream, the sphere-cone shock wave has the inflection point caused by the overexpansion-recompression region, and the hyperboloid shock shape exhibits its typical smoothness.

Comparisons between measured and predicted shock shapes on the sphere-cone and hyperboloid are presented in figures 14 and 15. For the sphere-cone at $\alpha = 0°$ and $5°$ (figs. 14(a) and (b)), there is excellent agreement between measured and predicted values. In the downstream regions of the sphere-cone for $\alpha = 10°$ (fig. 14(c)), the shock-shape overprediction is the result of a breakdown in the theory at this angle of attack, as noted previously with the pressure comparisons.

Comparisons between measured and predicted hyperboloid shock shapes for $\alpha = 0°$, $5°$, and $10°$ (figs. 15(a), (b), and (c)) show generally excellent agreement. For $\alpha = 15°$ (fig. 15(d)), the disagreement is due to the invalidity of the prediction technique for this case.

CONCLUDING REMARKS

An investigation was conducted to examine the measured and predicted pressure distributions, forces and moments, and shock shapes for a geometrically matched sphere-cone and hyperboloid. All tests were performed in the 22-inch aerodynamics leg of the Langley Hypersonic Helium Tunnel Facility at a Mach number of 20.3. Predicted values were obtained by using a theoretical method by Kumar and Graves (AIAA Paper No. 77-172).

Results from the measured and predicted pressure distributions showed much smoother variations for the hyperboloid than for the sphere-cone. Besides showing better agreement with measured pressures on the hyperboloid, the prediction method also provided better results at higher angles of attack on the hyperboloid than on the sphere-cone. Aside from the approximately 4 percent higher drag coefficient (near $\alpha = 0°$) for the sphere-cone, little or no difference existed in the measured and predicted static aerodynamic coefficients. Also, essentially no difference in the measured longitudinal stability was noted for the two shapes for angles of attack up to approximately 18°. Shock-shape measurements (which are less sensitive parameters for comparison purposes) also produced similar findings. The measured and predicted shock shapes were much smoother for the hyperboloid than for the sphere-cone, and the prediction method provided better results at higher angles of attack on the hyperboloid than on the sphere-cone.

It was shown in this investigation that the geometrically matched sphere-cone and hyperboloid were approximately identical in shape and, therefore, in volume. Physically, then, the hyperboloid shape could replace the sphere-cone. Measurements which helped determine the performance of the two shapes have also been made and showed little or no difference. As expected, because of its analytical nature, predictions for the hyperboloid provided better agreement with measured values and also provided better results for higher angles of attack. Since the final design of planetary entry probes depends on prediction methods, greater consideration should be given to hyperboloid shapes for planetary missions.

Langley Research Center
National Aeronautics and Space Administration
Hampton, VA 23665
November 19, 1982

REFERENCES

1. Arnold, John W.; Simmons, Harmon L.; and Miller, William T.: An Investigation of the Aerodynamic Characteristics of a 25° Sphere-Cone Including a Pressure Distribution Analysis at Angles of Attack, and a Trajectory Analysis During a Typical Reentry Trajectory. Contract No. NAS1-3915, LTV Aerosp. Corp., [1966]. (Available as NASA CR-66037.)

2. Foster, A. D., compiler: A Compilation of Longitudinal Aerodynamic Characteristics Including Pressure Information for Sharp- and Blunt-Nose Cones Having Flat and Modified Bases. SC-R-64-1311, Sandia Corp., Jan. 1965.

3. Geudtner, W. J., Jr.: Sharp and Blunted Cone Force Coefficients and Centers of Pressure From Wind Tunnel Tests at Mach Numbers From 0.50 to 4.06. Rep. No. ZA-7-017, Convair, June 16, 1955.

4. Machell, Reginald M.; and O'Bryant, William T.: An Experimental Investigation of the Flow Over Blunt-Nosed Cones at a Mach Number of 5.8. GALCIT Memo. No. 32 (Contract No. DA-04-495-Ord-19), June 15, 1956.

5. Zakkay, Victor: Pressure and Laminar Heat Transfer Results in Three-Dimensional Hypersonic Flow. WADC Tech. Note 58-182, DTIC Doc. No. AD 155 679, U.S. Air Force, Sept. 1958.

6. Armstrong, William O.: Hypersonic Aerodynamic Characteristics of Several Series of Lifting Bodies Appplicable to Reentry Vehicle Design. NASA TM X-536, 1961.

7. Ladson, Charles L.; Blackstock, Thomas A.; and Baradell, Donald L.: Air-Helium Simulation of the Aerodynamic Force Coefficients of Cones at Hypersonic Speeds. NASA TN D-1473, 1962.

8. Keyes, J. Wayne: Longitudinal Aerodynamic Characteristics of Blunted Cones at Mach Numbers of 3.5, 4.2, and 6.0. NASA TN D-2201, 1964.

9. Cleary, Joseph W.: An Experimental and Theoretical Investigation of the Pressure Distribution and Flow Fields of Blunted Cones at Hypersonic Mach Numbers. NASA TN D-2969, 1965.

10. Owens, Robert V.: Aerodynamic Characteristics of Spherically Blunted Cones at Mach Numbers From 0.5 to 5.0. NASA TN D-3088, 1965.

11. Treon, Stuart L.: Static Aerodynamic Characteristics of Short Blunt Cones With Various Nose and Base Cone Angles at Mach Numbers From 0.6 to 5.5 and Angles of Attack to 180°. NASA TN D-1327, 1962.

12. Nichols, James; and Nierengarten, Edward: Static Aerodynamic Characteristics of Blunted Cones and Round-Shouldered Cylinders Suitable for Planetary Entry Vehicles at a Mach-Number Range 1.65 to 9.00. WT 20-558, Jet Propul. Lab., California Inst. Technol., Feb. 15, 1964. (Available as NASA CR-58666.)

13. Penland, Jim A.: Aerodynamic Force Characteristics of a Series of Lifting Cone and Cone-Cylinder Configurations at a Mach Number of 6.83 and Angles of Attack up to 130°. NASA TN D-840, 1961.

14. Harris, Julius E.: Aerodynamic Characteristics of a Spherically Blunted 25° Cone at a Mach Number of 20. NASA TN D-4098, 1967.

15. Bushnell, Dennis M.; Jones, Robert A.; and Huffman, Jarrett K.: Heat-Transfer and Pressure Distributions on Spherically Blunted 25° Half-Angle Cone at Mach 8 and Angles of Attack up to 90°. NASA TN D-4792, 1968.

16. Campbell, James F.; and Howell, Dorothy T.: Supersonic Aerodynamics of Large-Angle Cones. NASA TN D-4719, 1968.

17. Campbell, James F.: Supersonic Aerodynamic Characteristics and Shock Standoff Distances for Large-Angle Cones With and Without Cylindrical Afterbodies. NASA TN D-5334, 1969.

18. Walker, Billy; and Weaver, Robert W.: Static Aerodynamic Characteristics of Blunted Cones in the Mach-Number Range From 2.2 to 9.5. Tech. Rep. 32-1213 (Contract No. NAS7-100), Jet Propul. Lab., California Inst. Technol., Dec. 1, 1967. (Available as NASA CR-94553.)

19. Blake, W. W.: Experimental Aerodynamic Characteristics of the Viking Entry Vehicle Over the Mach Range 1.5 - 10.0. TR-3720106 (Contract No. NAS1-9000), Martin Marietta Corp., Apr. 1971. (Available as NASA CR-159225.)

20. Emunds, Hans: Aerodynamic Coefficients and Position of the Bow Shock Wave of Circular Cones With Pointed and Spherically Blunted Noses in Supersonic Flow. ESA TT-335, Oct. 1976.

21. Intrieri, Peter F.; DeRose, Charles E.; and Kirk, Donn B.: Flight Characteristics of Probes in the Atmospheres of Mars, Venus, and the Outer Planets. IAF-76-076, Oct. 1976.

22. Calloway, Robert L.; and White, Nancy H.: Measured and Predicted Shock Shapes and Aerodynamic Coefficients for Blunted Cones at Incidence in Air at Mach 5.9. NASA TP-1652, 1980.

23. Maddalon, Dal V.: Aerodynamic Characteristics of the Sharp Right Circular Cone at Mach 20.3 and Angles of Attack to 110° in Helium. NASA TN D-3201, 1966.

24. Stewart, David A.; and Inouye, Mamoru: Shock Shapes and Pressure Distributions for Large-Angle Pointed Cones in Helium at Mach Numbers of 8 and 20. NASA TN D-5343, 1969.

25. Cleary, Joseph W.; and Duller, Charles E.: Effects of Angle of Attack and Bluntness on the Hypersonic Flow Over a 15° Semiapex Cone in Helium. NASA TN D-5903, 1970.

26. Jones, Robert A.; and Hunt, James L.: Measured Pressure Distributions on Large-Angle Cones in Hypersonic Flows of Tetrafluoromethane, Air, and Helium. NASA TN D-7429, 1973.

27. Miller, Charles G., III: Shock Shapes on Blunt Bodies in Hypersonic-Hypervelocity Helium, Air, and CO_2 Flows, and Calibration Results in Langley 6-Inch Expansion Tube. NASA TN D-7800, 1975.

28. Calloway, Robert L.; and White, Nancy H.: Measured and Predicted Shock Shapes and Aerodynamic Coefficients for Blunted Cones at Incidence in Helium at Mach 20.3. NASA TP-1395, 1979.

29. Olstad, Walter B.: Developing a Technology Base in Planetary Entry Aerothermodynamics. Space Activity - Impact on Science and Technology, P. Contensou and W. F. Hilton, eds., Pergamon Press, Inc., c.1976, pp. 257-291.

30. Kumar, Ajay; and Graves, R. A., Jr.: Numerical Solution of the Viscous Hypersonic Flow Past Blunted Cones at Angle of Attack. AIAA Paper No. 77-172, Jan. 1977.

31. Arrington, James P.; Joiner, Roy C., Jr.; and Henderson, Arthur, Jr.: Longitudinal Characteristics of Several Configurations at Hypersonic Mach Numbers in Conical and Contoured Nozzles. NASA TN D-2489, 1964.

32. Woods, William C.; and Arrington, James P.: Electron-Beam Flow Visualization - Applications in the Definition of Configuration Aerothermal Characteristics. AIAA Paper No. 72-1016, Sept. 1972.

33. Kumar, Ajay; and Graves, R. A., Jr.: A Vectorized Code for Calculating Laminar and Turbulent Hypersonic Flows About Blunt Axisymmetric Bodies at Zero and Small Angles of Attack. NASA TM-80202, 1980.

34. Watson, Ralph D.: Wall Cooling Effects on Hypersonic Transitional/Turbulent Boundary Layers at High Reynolds Numbers. AIAA Paper No. 75-834, June 1975.

TABLE I.- MEASURED SPHERE-CONE PRESSURES (p/2q)

$\phi = 0°$

s/s_t	$\alpha = 0°$	$\alpha = 5°$	$\alpha = 10°$	$\alpha = 15°$	$\alpha = 18°$
0.000	.8189	.8183	.8059	.7825	.7628
.064	.8049	.7934	.7543	.7024	.6645
.128	.7601	.7219	.6648	.5938	.5497
.191	.6570	.5869	.5172	.4436	.4001
.255	.5242	.4471	.3801	.3141	.2787
.319	.4881	.3934	.2931	.2276	.1956
.382	.5000	.3932	.3054	.2332	.1993
.445	.5258	.4102	.3170	.2410	.2050
.509	.5312	.4231	.3270	.2471	.2104
.573	.5488	.4370	.3378	.2522	.2134
.637	.5515	.4464	.3481	.2576	.2170
.700	.5625	.4515	.3537	.2602	.2167
.764	.5617	.4583	.3606	.2640	.2191
.828	.5672	.4579	.3589	.2625	.2151
.892	.5570	.4562	.3583	.2614	.2132
.956	.5312	.4309	.3345	.2416	.1935

$\phi = 22.5°$

s/s_t	$\alpha = 0°$	$\alpha = 5°$	$\alpha = 10°$	$\alpha = 15°$	$\alpha = 18°$
0.000	.8201	.8161	.8052	.7837	.7632
.064	.8084	.7930	.7584	.7093	.6723
.128	.7508	.7154	.6623	.5962	.5570
.191	.6495	.5891	.5242	.4552	.4138
.255	.5213	.4517	.3857	.3214	.2885
.319	.4777	.3844	.3075	.2449	.2132
.382	.5001	.4031	.3193	.2503	.2181
.445	.5158	.4189	.3318	.2606	.2245
.509	.5306	.4330	.3405	.2616	.2258
.573	.5385	.4438	.3492	.2661	.2280
.637	.5512	.4545	.3586	.2681	.2279
.700	.5527	.4585	.3640	.2727	.2280
.764	.5605	.4653	.3702	.2747	.2307
.828	.5552	.4632	.3709	.2781	.2302
.892	.5558	.4631	.3704	.2772	.2309
.956	.5152	.4338	.3497	.2659	.2177

TABLE I.- Continued

ϕ = 45°

s/s_t	α = 0°	α = 5°	α = 10°	α = 15°	α = 18°
0.000	.8201	.8199	.8064	.7817	.7633
.064	.8076	.7977	.7671	.7222	.6898
.128	.7478	.7188	.6759	.6213	.5811
.191	.6469	.6013	.5459	.4868	.4515
.255	.5187	.4633	.4103	.3560	.3224
.319	.4787	.4090	.3498	.2995	.2717
.382	.4977	.4230	.3603	.3050	.2720
.445	.5170	.4435	.3739	.3130	.2792
.509	.5288	.4525	.3801	.3131	.2754
.573	.5387	.4655	.3879	.3156	.2768
.637	.5484	.4722	.3951	.3176	.2750
.700	.5524	.4785	.3998	.3199	.2763
.764	.5574	.4824	.4057	.3227	.2755
.828	.5531	.4819	.4053	.3221	.2746
.892	.5525	.4797	.4061	.3224	.2729
.956	.5114	.4492	.3808	.3028	.2558

ϕ = 67.5°

s/s_t	α = 0°	α = 5°	α = 10°	α = 15°	α = 18°
0.000	.8209	.8169	.8048	.7819	.7653
.064	.8060	.8009	.7795	.7450	.7196
.128	.7479	.7285	.6950	.6422	.6249
.191	.6438	.6181	.5817	.5395	.5128
.255	.5132	.4830	.4484	.4128	.3904
.319	.4771	.4404	.4116	.3839	.3651
.382	.4945	.4536	.4147	.3771	.3546
.445	.5151	.4752	.4351	.3926	.3649
.509	.5264	.4831	.4336	.3824	.3524
.573	.5365	.4949	.4462	.3916	.3579
.637	.5482	.5011	.4466	.3846	.3482
.700	.5470	.5062	.4536	.3914	.3535
.764	.5555	.5101	.4539	.3862	.3459
.828	.5477	.5080	.4556	.3901	.3496
.892	.5465	.5063	.4512	.3818	.3394
.956	.5078	.4719	.4272	.3622	.3222

TABLE I.- Continued

$\phi = 90°$

s/s_t	$\alpha = 0°$	$\alpha = 5°$	$\alpha = 10°$	$\alpha = 15°$	$\alpha = 18°$
0.000	.8225	.8162	.8055	.7806	.7642
.064	.8069	.8072	.7941	.7649	.7471
.128	.7601	.7430	.7275	.6966	.6800
.191	.6433	.6410	.6311	.6084	.5924
.255	.5136	.5123	.5106	.5019	.4934
.319	.4752	.4807	.4887	.4832	.4755
.382	.4936	.4913	.4882	.4714	.4581
.445	.5120	.5127	.5068	.4834	.4658
.509	.5261	.5203	.5057	.4747	.4527
.573	.5337	.5317	.5162	.4814	.4582
.637	.5475	.5383	.5167	.4762	.4494
.700	.5453	.5425	.5212	.4789	.4520
.764	.5544	.5488	.5200	.4735	.4445
.828	.5459	.5426	.5176	.4714	.4422
.892	.5479	.5402	.5106	.4607	.4300
.956	.5070	.5033	.4785	.4323	.4027

$\phi = 112.5°$

s/s_t	$\alpha = 0°$	$\alpha = 5°$	$\alpha = 10°$	$\alpha = 15°$	$\alpha = 18°$
0.000	.8216	.8152	.8017	.7793	.7621
.064	.8068	.8102	.8035	.7865	.7760
.128	.7777	.7669	.7607	.7444	.7339
.191	.6478	.6675	.6824	.6861	.6833
.255	.5194	.5496	.5836	.6035	.6068
.319	.4747	.5217	.5683	.5910	.5947
.382	.4939	.5308	.5679	.5756	.5703
.445	.5121	.5556	.5834	.5860	.5804
.509	.5278	.5628	.5843	.5781	.5676
.573	.5340	.5733	.5916	.5841	.5745
.637	.5490	.5797	.5921	.5781	.5660
.700	.5454	.5833	.5934	.5798	.5679
.764	.5572	.5863	.5903	.5704	.5562
.828	.5465	.5819	.5845	.5648	.5500
.892	.5519	.5770	.5721	.5473	.5298
.956	.5077	.5396	.5348	.5059	.4913

TABLE I.- Continued

ϕ = 135°

s/s_t	α = 0°	α = 5°	α = 10°	α = 15°	α = 18°
0.000	.8201	.8118	.8041	.7822	.7597
.064	.8079	.8098	.8134	.8051	.7965
.128	.7823	.7929	.7927	.7808	.7788
.191	.6556	.6946	.7327	.7545	.7567
.255	.5232	.5881	.6579	.7035	.7087
.319	.4763	.5594	.6376	.6853	.6962
.382	.4949	.5721	.6399	.6748	.6817
.445	.5136	.5899	.6515	.6822	.6863
.509	.5279	.5991	.6510	.6717	.6778
.573	.5360	.6072	.6576	.6797	.6837
.637	.5495	.6132	.6529	.6666	.6705
.700	.5493	.6150	.6539	.6622	.6719
.764	.5578	.6173	.6460	.6531	.6552
.828	.5509	.6103	.6380	.6448	.6470
.892	.5520	.6036	.6203	.6197	.6203
.956	.5116	.5620	.5742	.5698	.5675

ϕ = 157.5°

s/s_t	α = 0°	α = 5°	α = 10°	α = 15°	α = 18°
0.000	.8204	.8144	.8025	.7781	.7614
.064	.8165	.8169	.8169	.8083	.8105
.128	.7815	.8062	.8176	.8087	.8107
.191	.6566	.7142	.7659	.7928	.8011
.255	.5268	.6143	.7080	.7790	.7911
.319	.4749	.5824	.6847	.7531	.7727
.382	.4983	.6010	.6911	.7506	.7728
.445	.5127	.6131	.6961	.7470	.7680
.509	.5304	.6265	.6994	.7447	.7622
.573	.5353	.6293	.6999	.7413	.7605
.637	.5511	.6387	.6985	.7360	.7514
.700	.5467	.6354	.6925	.7269	.7453
.764	.5593	.6407	.6870	.7179	.7325
.828	.5482	.6284	.6713	.6983	.7153
.892	.5529	.6232	.6548	.6773	.6896
.956	.5098	.5756	.5989	.6121	.6237

TABLE I.- Concluded

$\phi = 180°$

s/s_t	$\alpha = 0°$	$\alpha = 5°$	$\alpha = 10°$	$\alpha = 15°$	$\alpha = 18°$
0.000	.8221	.8157	.8063	.7822	.7628
.064	.8245	.8198	.8182	.8123	.8147
.128	.7714	.7991	.8154	.8172	.8248
.191	.6595	.7249	.7860	.8226	.8158
.255	.5135	.6200	.7216	.7937	.8088
.319	.4774	.5922	.6993	.7777	.8004
.382	.4854	.6101	.7068	.7728	.8003
.445	.5122	.6247	.7124	.7712	.7931
.509	.5166	.6343	.7148	.7674	.7918
.573	.5385	.6411	.7150	.7642	.7845
.637	.5343	.6457	.7132	.7580	.7804
.700	.5515	.6464	.7072	.7497	.7687
.764	.5455	.6465	.6992	.7376	.7600
.828	.5526	.6381	.6842	.7195	.7388
.892	.5363	.6275	.6649	.6944	.7145
.956	.5123	.5838	.6091	.6295	.6436

TABLE II.- MEASURED HYPERBOLOID PRESSURES (p/2q)

$\phi = 0°$

s/s_t	$\alpha = 0°$	$\alpha = 5°$	$\alpha = 10°$	$\alpha = 15°$	$\alpha = 18°$
0.000	.8208	.8148	.7959	.7693	.7430
.085	.7869	.7511	.6934	.6221	.5751
.126	.7526	.6986	.6264	.5446	.4962
.180	.6977	.6265	.5448	.4631	.4167
.230	.6586	.5799	.4945	.4105	.3666
.276	.6247	.5430	.4582	.3778	.3333
.318	.6001	.5151	.4305	.3497	.3076
.359	.5793	.4927	.4085	.3251	.2874
.436	.5543	.4651	.3799	.3006	.2597
.512	.5318	.4431	.3587	.2824	.2405
.586	.5169	.4270	.3422	.2649	.2260
.657	.5053	.4154	.3304	.2555	.2155
.729	.4982	.4065	.3205	.2437	.2060
.799	.4933	.4016	.3150	.2395	.1996
.869	.4955	.4034	.3155	.2362	.1973
.939	.4787	.3925	.3069	.2306	.1900

$\phi = 22.5°$

s/s_t	$\alpha = 0°$	$\alpha = 5°$	$\alpha = 10°$	$\alpha = 15°$	$\alpha = 18°$
0.000	.8222	.8155	.7964	.7668	.7396
.085	.7920	.7552	.6975	.6284	.5811
.126	.7418	.6937	.6248	.5524	.5074
.180	.6975	.6315	.5527	.4717	.4287
.230	.6519	.5814	.4996	.4229	.3666
.276	.6238	.5500	.4690	.3919	.3475
.318	.5955	.5177	.4365	.3616	.3208
.359	.5792	.5010	.4193	.3434	.2999
.436	.5493	.4690	.3876	.3127	.2729
.512	.5320	.4512	.3690	.2943	.2523
.586	.5145	.4319	.3506	.2767	.2385
.657	.5051	.4225	.3402	.2665	.2266
.729	.4959	.4117	.3285	.2551	.2177
.799	.4910	.4079	.3244	.2499	.2094
.869	.4933	.4085	.3226	.2470	.2091
.939	.4747	.3963	.3146	.2401	.1993

TABLE II.- Continued

$\phi = 45°$

s/s_t	$\alpha = 0°$	$\alpha = 5°$	$\alpha = 10°$	$\alpha = 15°$	$\alpha = 18°$
0.000	.8205	.8128	.7929	.7635	.7411
.085	.7856	.7572	.7093	.6484	.6094
.126	.7414	.7030	.6462	.5800	.5398
.180	.6908	.6391	.5754	.5074	.4683
.230	.6523	.5923	.5294	.4593	.4202
.276	.6173	.5606	.4956	.4294	.3919
.318	.5961	.5343	.4669	.3986	.3612
.359	.5736	.5128	.4477	.3813	.3437
.436	.5521	.4870	.4195	.3513	.3141
.512	.5269	.4642	.3984	.3324	.2950
.586	.5163	.4507	.3827	.3144	.2779
.657	.4998	.4356	.3694	.3036	.2669
.729	.4972	.4301	.3607	.2920	.2559
.799	.4846	.4198	.3525	.2854	.2485
.869	.4944	.4267	.3226	.2840	.2467
.939	.4661	.4055	.3399	.2730	.2365

$\phi = 67.5°$

s/s_t	$\alpha = 0°$	$\alpha = 5°$	$\alpha = 10°$	$\alpha = 15°$	$\alpha = 18°$
0.000	.8203	.8109	.7929	.7622	.7386
.085	.7843	.7657	.7300	.6816	.6566
.126	.7396	.7136	.6747	.6235	.5888
.180	.6865	.6563	.6136	.5603	.5259
.230	.6478	.6155	.5722	.5180	.4844
.276	.6138	.5812	.5374	.4885	.4570
.318	.5916	.5564	.5105	.4590	.4272
.359	.5707	.5342	.4918	.4426	.4115
.436	.5464	.5093	.4660	.4148	.3830
.512	.5237	.4876	.4442	.3952	.3636
.586	.5140	.4754	.4317	.3793	.3464
.657	.4972	.4599	.4156	.3659	.3340
.729	.4937	.4544	.4099	.3567	.3235
.799	.4815	.4438	.3987	.3473	.3145
.869	.4900	.4503	.4042	.3482	.3134
.939	.4631	.4273	.3827	.3319	.2984

TABLE II.- Continued

$\phi = 90°$

s/s_t	$\alpha = 0°$	$\alpha = 5°$	$\alpha = 10°$	$\alpha = 15°$	$\alpha = 18°$
0.000	.8165	.8117	.7950	.7668	.7356
.085	.7839	.7806	.7584	.7250	.6902
.126	.7491	.7338	.7112	.6788	.6483
.180	.6887	.6832	.6630	.6320	.6020
.230	.6494	.6429	.6238	.5944	.5672
.276	.6156	.6114	.5948	.5678	.5417
.318	.5901	.5851	.5677	.5386	.5141
.359	.5722	.5680	.5518	.5241	.5003
.436	.5440	.5397	.5237	.4988	.4750
.512	.5229	.5093	.5045	.4798	.4565
.586	.5118	.5079	.4918	.4664	.4432
.657	.4973	.4934	.4776	.4511	.4274
.729	.4914	.4877	.4712	.4440	.4202
.799	.4810	.4769	.4597	.4316	.4070
.869	.4868	.4827	.4634	.4319	.4058
.939	.4635	.4583	.4400	.4093	.3824

$\phi = 112.5°$

s/s_t	$\alpha = 0°$	$\alpha = 5°$	$\alpha = 10°$	$\alpha = 15°$	$\alpha = 18°$
0.000	.8180	.8102	.7905	.7636	.7387
.085	.7864	.7908	.7813	.7621	.7449
.126	.7665	.7614	.7507	.7282	.7127
.180	.6936	.7072	.7132	.7025	.6901
.230	.6585	.6766	.6833	.6731	.6593
.276	.6176	.6426	.6527	.6503	.6411
.318	.5954	.6180	.6309	.6277	.6160
.359	.5725	.6004	.6142	.6150	.6073
.436	.5476	.5749	.5910	.5919	.5827
.512	.5228	.5565	.5738	.5776	.5707
.586	.5139	.5437	.5615	.5635	.5557
.657	.4969	.5281	.5455	.5501	.5418
.729	.4934	.5214	.5415	.5413	.5329
.799	.4803	.5116	.5272	.5270	.5186
.869	.4900	.5160	.5284	.5205	.5084
.939	.4633	.4919	.5013	.4901	.4773

TABLE II.- Continued

ϕ = 135°

s/s_t	α = 0°	α = 5°	α = 10°	α = 15°	α = 18°
0.000	.8204	.8126	.7919	.7645	.7392
.085	.7894	.7993	.8002	.7922	.7870
.126	.7709	.7927	.7934	.7731	.7668
.180	.6996	.7375	.7581	.7635	.7621
.230	.6622	.7113	.7446	.7587	.7423
.276	.6224	.6734	.7100	.7284	.7295
.318	.5984	.6520	.6926	.7198	.7221
.359	.5756	.6313	.6751	.7019	.7052
.436	.5511	.6078	.6522	.6836	.6926
.512	.5248	.5869	.6361	.6692	.6786
.586	.5136	.5740	.6212	.6538	.6635
.657	.4975	.5602	.6097	.6418	.6527
.729	.4953	.5566	.6027	.6318	.6401
.799	.4808	.5410	.5889	.6147	.6229
.869	.4884	.5476	.5843	.6032	.6069
.939	.4650	.5180	.5522	.5605	.5623

ϕ = 157.5°

s/s_t	α = 0°	α = 5°	α = 10°	α = 15°	α = 18°
0.000	.8168	.8086	.7891	.7625	.7383
.085	.7937	.8033	.8094	.8101	.8106
.126	.7707	.8046	.8161	.8076	.8020
.180	.7016	.7533	.7901	.8028	.8024
.230	.6649	.7301	.7824	.8153	.8053
.276	.6230	.6915	.7497	.7917	.7931
.318	.6013	.6731	.7368	.7862	.8129
.359	.5761	.6496	.7142	.7695	.7863
.436	.5540	.6288	.6973	.7513	.7728
.512	.5268	.6074	.6771	.7333	.7575
.586	.5152	.5953	.6669	.7220	.7429
.657	.4993	.5812	.6514	.7089	.7310
.729	.4938	.5746	.6448	.6958	.7159
.799	.4834	.5637	.6297	.6785	.6982
.869	.4869	.5654	.6235	.6601	.6747
.939	.4668	.5373	.5825	.6107	.6230

TABLE II.- Concluded

$\phi = 180°$

s/s_t	$\alpha = 0°$	$\alpha = 5°$	$\alpha = 10°$	$\alpha = 15°$	$\alpha = 18°$
0.000	.8176	.8131	.7948	.7615	.7379
.085	.8009	.8128	.8163	.8094	.8161
.126	.7660	.7970	.8233	.8183	.8231
.180	.7036	.7661	.8103	.8230	.8157
.230	.6626	.7316	.7932	.8235	.8183
.276	.6229	.7013	.7672	.8155	.8252
.318	.5997	.6777	.7507	.8064	.8215
.359	.5757	.6595	.7328	.7906	.8139
.436	.5521	.6349	.7137	.7739	.8011
.512	.5275	.6176	.6954	.7559	.7819
.586	.5133	.5987	.6841	.7460	.7721
.657	.5060	.5910	.6705	.7302	.7568
.729	.4921	.5804	.6609	.7190	.7440
.799	.4845	.5746	.6478	.6992	.7236
.869	.4848	.5692	.6369	.6811	.7016
.939	.4676	.5470	.5971	.6277	.6448

TABLE III.- MEASURED SPHERE-CONE SHOCK SHAPES

$\alpha = 0°$		$\alpha = 5°$	
x/r_b	r/r_b	x/r_b	r/r_b
-.1097	.0008	-.1040	.0017
-.1054	.0982	-.0984	.0976
-.0844	.2030	-.0808	.1973
-.0393	.3026	-.0432	.3007
.0141	.4059	.0024	.4000
.0837	.5085	.0640	.4990
.1572	.6068	.1376	.5978
.2392	.7129	.2272	.7004
.3210	.8149	.3088	.7991
.3947	.9173	.3944	.9017
.4724	1.0195	.4681	1.0045
.5378	1.1182	.5497	1.1072
.6117	1.2247	.6274	1.2100
.6852	1.3230	.6929	1.3089
-.1097	.0008	-.0976	-.0984
-.0984	-.1094	-.0752	-.1988
-.0823	-.2036	-.0369	-.3034
-.0343	-.3115	.0256	-.4004
.0066	-.3987	.0800	-.5013
.0747	-.5115	.1464	-.6023
.1515	-.6125	.2207	-.7035
.2283	-.7135	.2831	-.8045
.3050	-.8145	.3536	-.9017
.3776	-.9193	.4200	-1.0027
.4544	-1.0203	.4784	-1.0997
.5230	-1.1209	.5568	-1.2009
.5878	-1.2173	.6232	-1.3020
.6644	-1.3224	.7095	-1.4034

TABLE III.- Continued

$\alpha = 10°$

x/r_b	r/r_b
-.1072	.0003
-.1060	.0956
-.0894	.1960
-.0612	.3012
-.0085	.3962
.0437	.4992
.1083	.5950
.1957	.7045
.2840	.8020
.3762	.8999
.4563	1.0008
.5448	1.0945
.6246	1.1994
.6895	1.2913
-.0998	-.1024
-.0804	-.2081
-.0499	-.3012
-.0028	-.4050
.0558	-.5039
.1187	-.6066
.1813	-.7053
.2439	-.8040
.3105	-.9024
.3770	-1.0008
.4523	-1.1105
.5265	-1.2045
.6089	-1.3017
.6957	-1.4067

$\alpha = 15°$

x/r_b	r/r_b
-.1124	.0003
-.1146	.1012
-.0960	.2056
-.0667	.3036
-.0297	.4000
.0204	.5016
.0821	.6007
.1514	.6981
.2254	.7985
.3139	.8918
.4087	.9957
.4989	1.0966
.5767	1.1962
.6669	1.2971
.7493	1.3997
-.0965	-.1116
-.0756	-.2005
-.0435	-.3118
.0034	-.4104
.0618	-.5114
.1104	-.6022
.1718	-.7079
.2349	-.8060
.3086	-.9103
.3772	-1.0015
.4633	-1.1045
.5502	-1.2037
.6486	-1.3053
.7517	-1.4040

TABLE III.- Concluded

$\alpha = 18°$

x/r_b	r/r_b
-.1160	0.0000
-.1215	.1006
-.1069	.2031
-.0808	.3004
-.0459	.4048
-.0075	.5048
.0467	.6031
.1097	.7086
.1845	.8128
.2550	.9135
.3453	1.0121
.4403	1.1182
.5345	1.2164
.6173	1.3198
-.1030	-.1053
-.0855	-.2071
-.0479	-.3070
-.0020	-.4038
.0479	-.5010
.1057	-.5990
.1706	-.7057
.2324	-.8042
.3100	-.9042
.3757	-1.0031
.4608	-1.1079
.5582	-1.2100
.6674	-1.3134

TABLE IV.- MEASURED HYPERBOLOID SHOCK SHAPES

$\alpha = 0°$

x/r_b	r/r_b
-.1076	-.0114
-.0984	.0964
-.0788	.1838
-.0388	.2868
.0013	.3744
.0465	.4620
.1019	.5600
.1576	.6324
.2080	.7200
.2535	.7821
.3142	.8648
.3750	.9423
.4407	1.0302
.5167	1.1232
.5927	1.2112
.6483	1.2887
-.1018	-.0728
-.0857	-.1445
-.0591	-.2416
-.0379	-.3081
-.0013	-.3744
.0303	-.4510
.0669	-.5224
.1190	-.6039
.1554	-.6548
.2128	-.7517
.2649	-.8281
.3326	-.9248
.4158	-1.0419
.5093	-1.1538
.5768	-1.2402
.6496	-1.3369

$\alpha = 5°$

x/r_b	r/r_b
-.0972	-.0028
-.0881	.0748
-.0745	.1579
-.0464	.2526
-.0220	.3315
.0175	.4116
.0571	.4918
.1263	.5847
.1574	.6436
.2025	.7191
.2633	.7908
.3330	.8786
.3878	.9600
.4389	1.0257
.4946	1.0969
.5507	1.1631
.6119	1.2296
.6816	1.3174
.7373	1.3887
-.0921	-.0639
-.0859	-.1403
-.0656	-.2002
-.0492	-.2758
-.0234	-.3403
.0126	-.4040
.0545	-.4775
.0960	-.5459
.1435	-.6241
.1786	-.6776
.2307	-.7502
.2714	-.8084
.3070	-.8671
.3599	-.9499
.4116	-1.0175
.4854	-1.1037
.5375	-1.1764
.5884	-1.2337
.6456	-1.3060
.6968	-1.3684

TABLE IV.- Continued

α = 10°		α = 15°	
x/r_b	r/r_b	x/r_b	r/r_b
-.1047	-.0038	-.1088	.0006
-.1050	.0751	-.1108	.0815
-.0972	.1340	-.0964	.1619
-.0806	.2047	-.0754	.2387
-.0440	.2834	-.0545	.3155
-.0229	.3600	-.0200	.4017
.0047	.4269	.0173	.4779
.0457	.5115	.0612	.5505
.0896	.5754	.1001	.6217
.1373	.6503	.1410	.7044
.1849	.7253	.1879	.7671
.2325	.8002	.2468	.8441
.2912	.8714	.2886	.9053
.3530	.9588	.3510	.9889
.4072	1.0241	.4049	1.0645
.4651	1.1005	.4518	1.1271
.5194	1.1658	.5086	1.1927
.5825	1.2428	.5619	1.2518
.6412	1.3140	.6137	1.3160
.7250	1.3939	-.1033	-.0738
-.0971	-.0975	-.0942	-.1417
-.0792	-.1897	-.0778	-.2347
-.0635	-.2665	-.0428	-.3169
-.0367	-.3471	-.0243	-.3984
.0063	-.4307	.0126	-.4391
.0486	-.5091	.0497	-.5397
.0895	-.5772	.0967	-.6074
.1297	-.6401	.1337	-.6781
.1698	-.7030	.1800	-.7458
.2159	-.7704	.2284	-.7970
.2613	-.8326	.2755	-.8647
.3125	-.8993	.3602	-.9866
.3651	-.9763	.4072	-1.0543
.4222	-1.0474	.4722	-1.1277
.4808	-1.1289	.5293	-1.1924
.5379	-1.2000	.5899	-1.2507
.5943	-1.2660	.6554	-1.3076
.6558	-1.3313		

TABLE IV.- Concluded

$\alpha = 18°$

x/r_b	r/r_b
-.1178	.0015
-.1153	.0638
-.1003	.1747
-.0699	.3073
-.0162	.4194
.0340	.5247
.0842	.6301
.1598	.7436
.2200	.8354
.2937	.9371
.3624	1.0372
.4447	1.1472
.5132	1.2304
.5901	1.3220
.6482	1.3852
-.1189	-.0825
-.1018	-.1888
-.0762	-.2868
-.0520	-.3629
-.0160	-.4408
.0248	-.5340
.0723	-.6306
.1382	-.7325
.2176	-.8413
.2870	-.9365
.3497	-1.0282
.4258	-1.1269
.5239	-1.2242
.6018	-1.3111
.6800	-1.3812

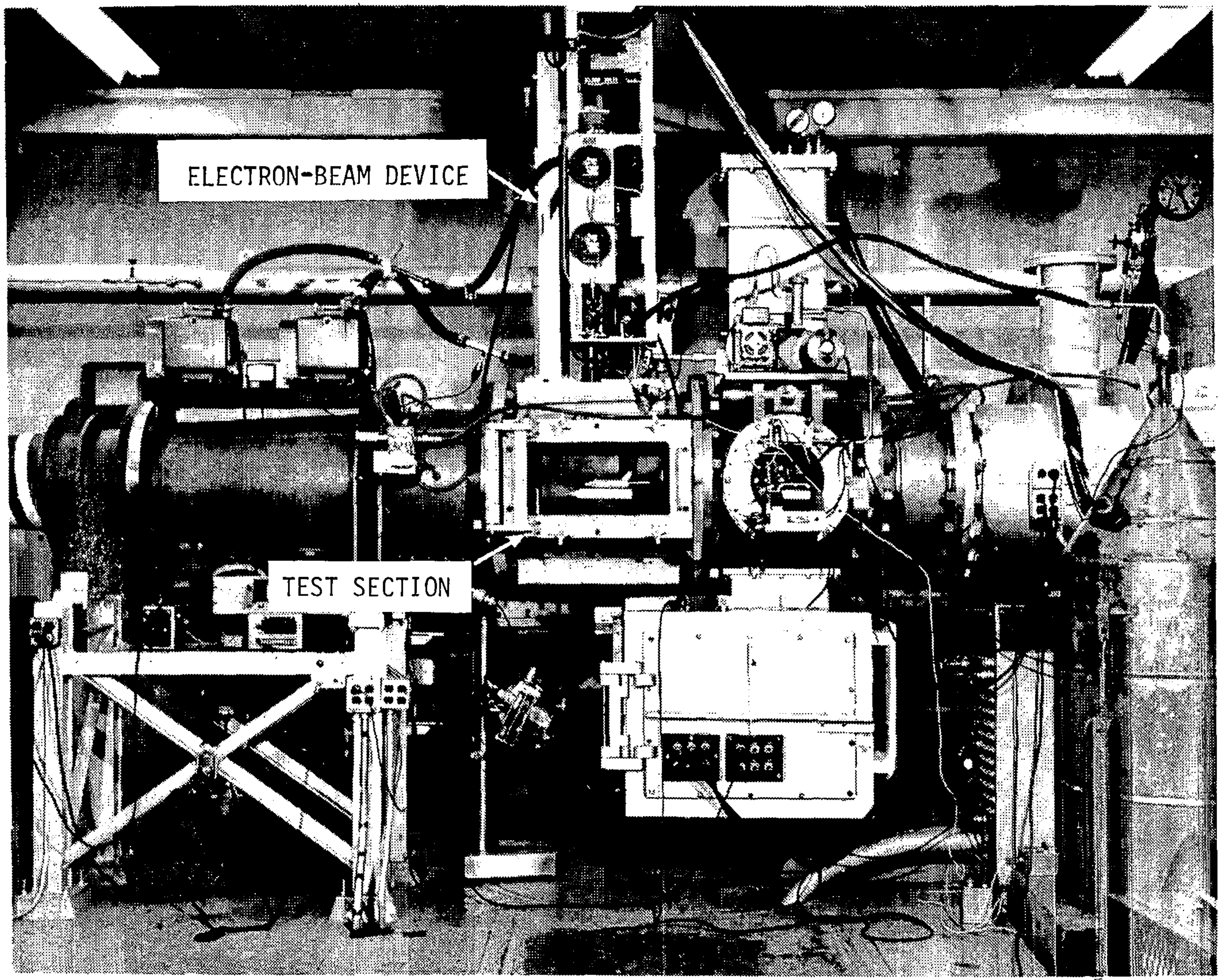

L-82-206

Figure 1.- Test area for the 22-inch aerodynamics leg of the Langley Hypersonic Helium Tunnel Facility.

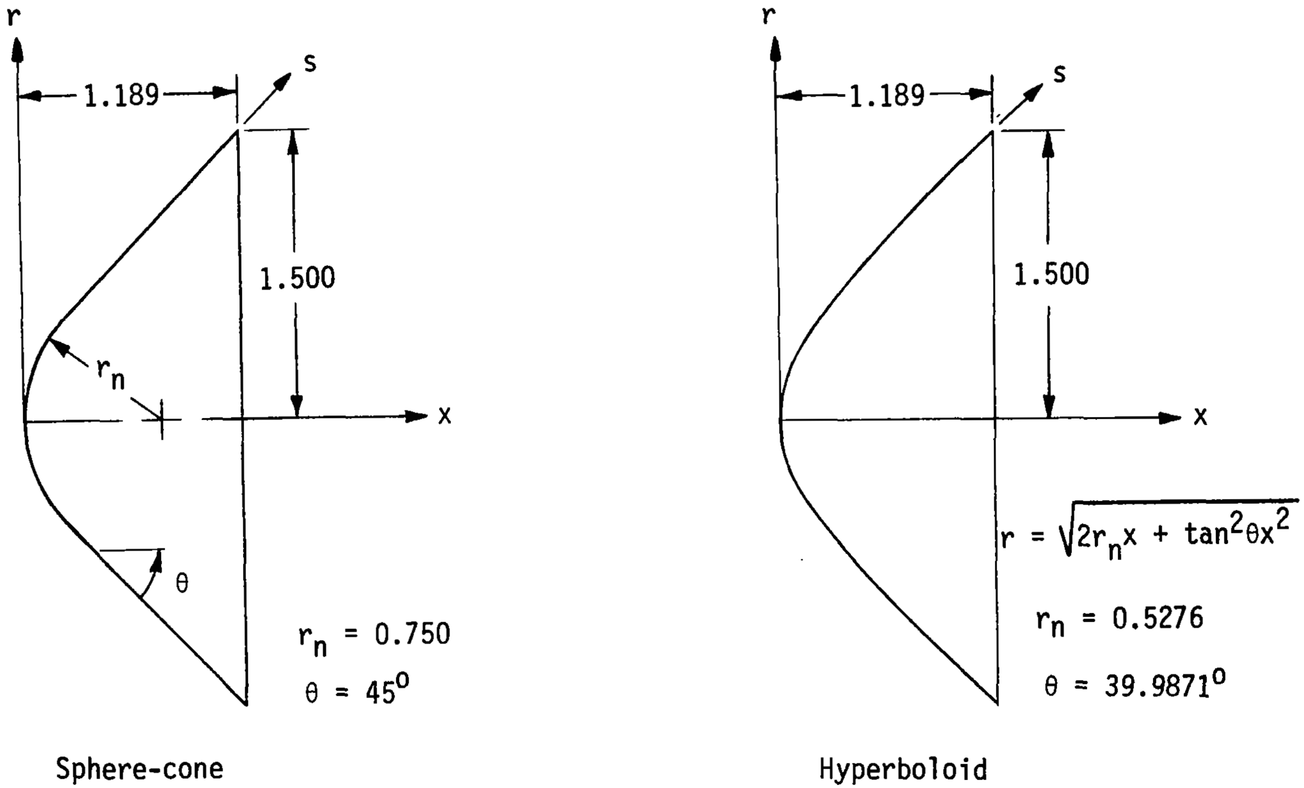

(a) Coordinate systems. (All dimensions in inches.)

Figure 2.- Sketch of sphere-cone and hyperboloid shapes.

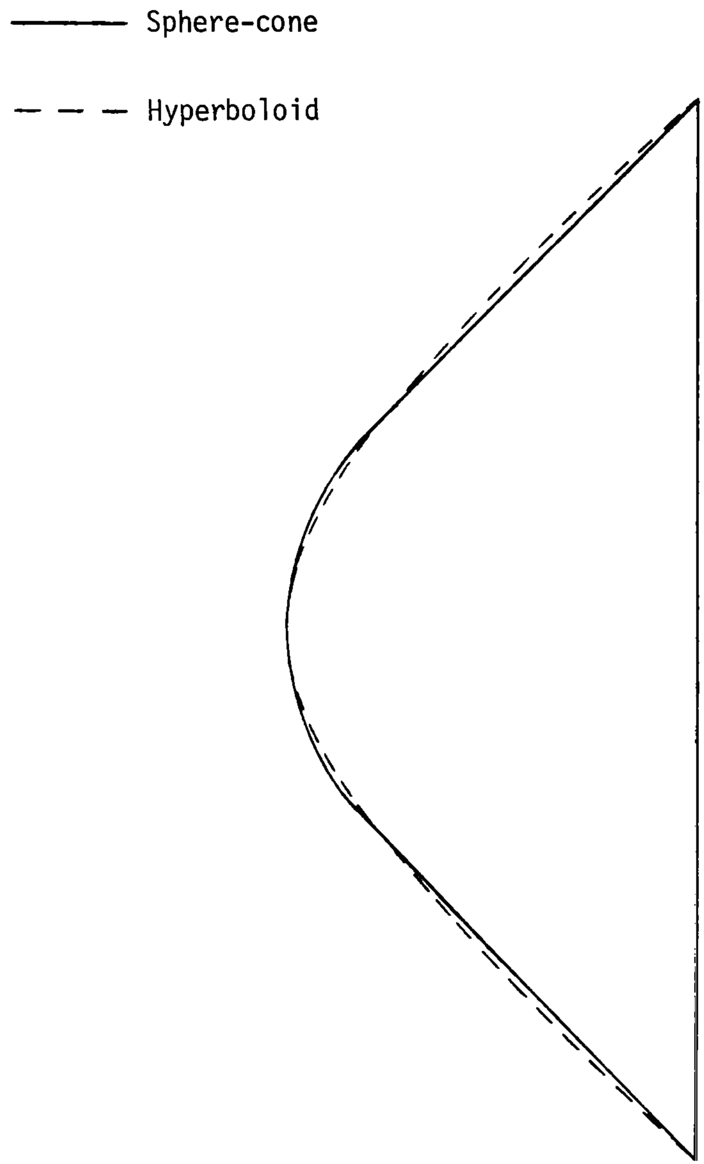

(b) Shape comparison.

Figure 2.- Concluded.

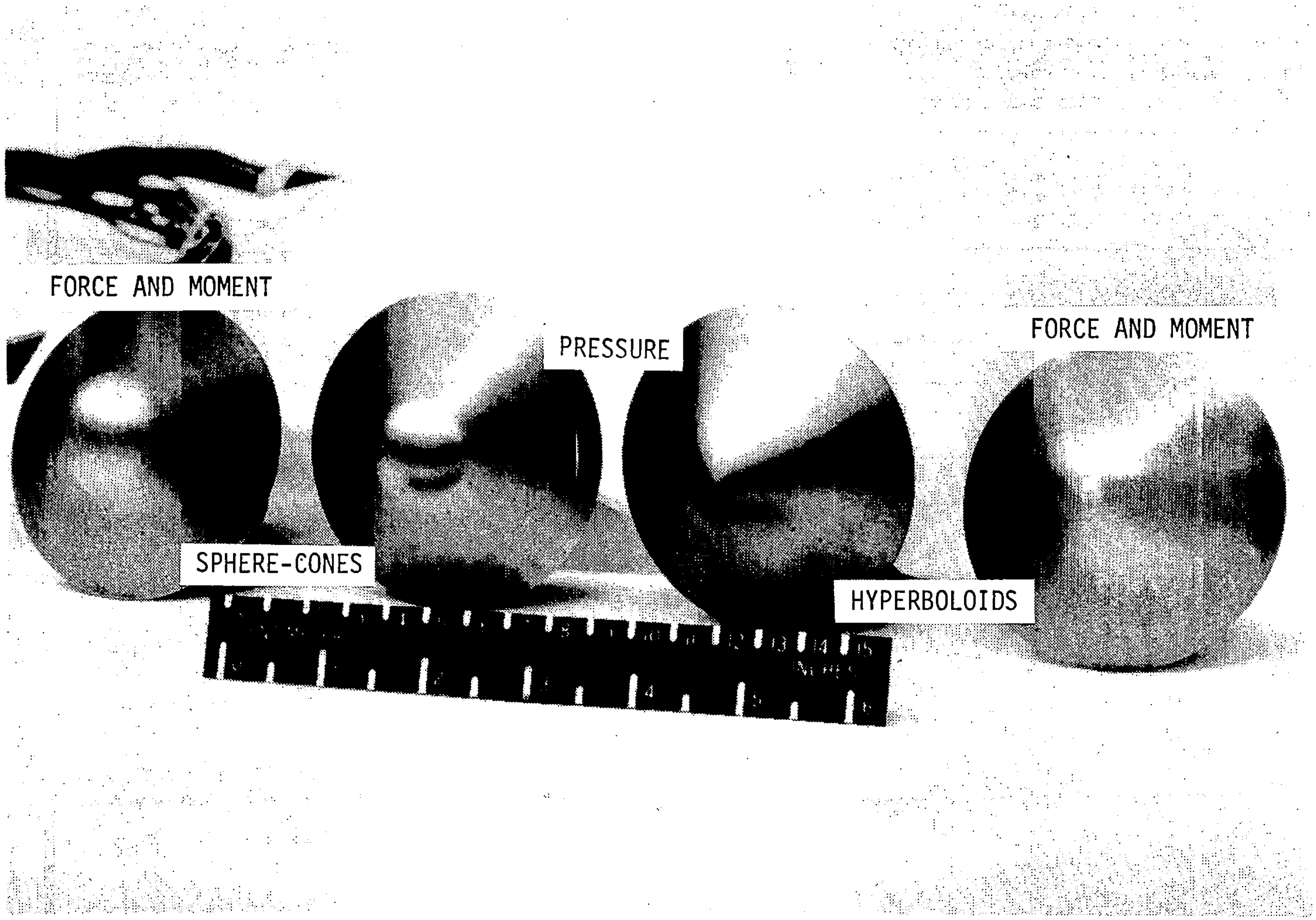

L-82-207

Figure 3.- Test models.

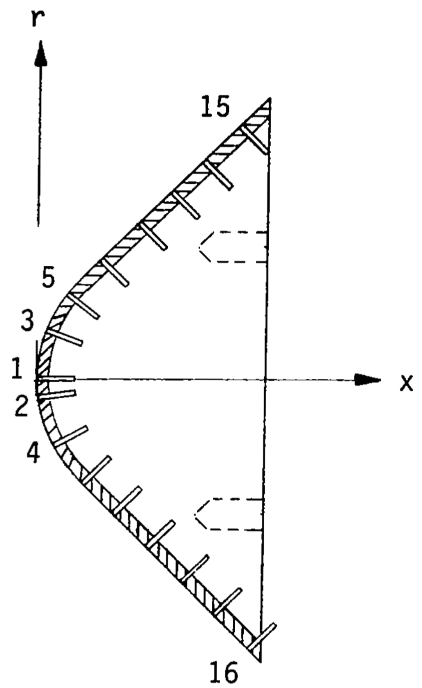

Orifice Number	x	r	s/s$_t$
1	0.0	0.0	0.0
2	0.010	0.124	0.064
3	0.041	0.245	0.128
4	0.092	0.360	0.191
5	0.161	0.464	0.255
6	0.245	0.556	0.319
7	0.334	0.644	0.382
8	0.422	0.733	0.445
9	0.510	0.821	0.509
10	0.599	0.909	0.573
11	0.687	0.998	0.637
12	0.776	1.086	0.700
13	0.864	1.175	0.764
14	0.952	1.263	0.828
15	1.041	1.351	0.892
16	1.129	1.440	0.956

(a) Sphere-cone.

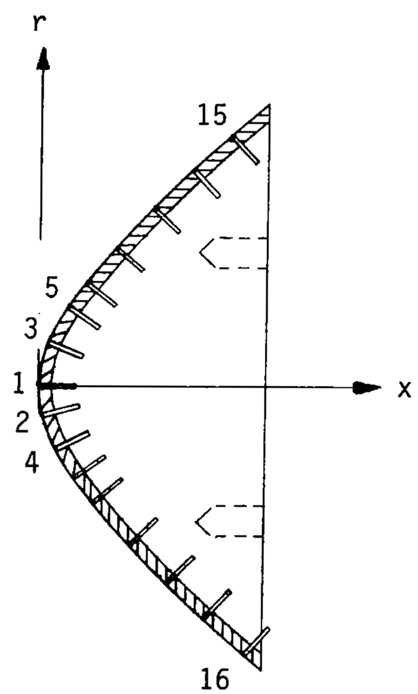

Orifice Number	x	r	s/s$_t$
1	0.0	0.0	0.0
2	0.025	0.164	0.085
3	0.050	0.234	0.126
4	0.100	0.336	0.180
5	0.150	0.417	0.230
6	0.200	0.489	0.276
7	0.250	0.555	0.318
8	0.300	0.616	0.359
9	0.400	0.731	0.436
10	0.500	0.839	0.512
11	0.600	0.942	0.586
12	0.700	1.041	0.657
13	0.800	1.138	0.729
14	0.900	1.233	0.799
15	1.000	1.326	0.869
16	1.100	1.418	0.939

(b) Hyperboloid.

Figure 4.- Sketch of pressure models with orifice locations. (All dimensions in inches.)

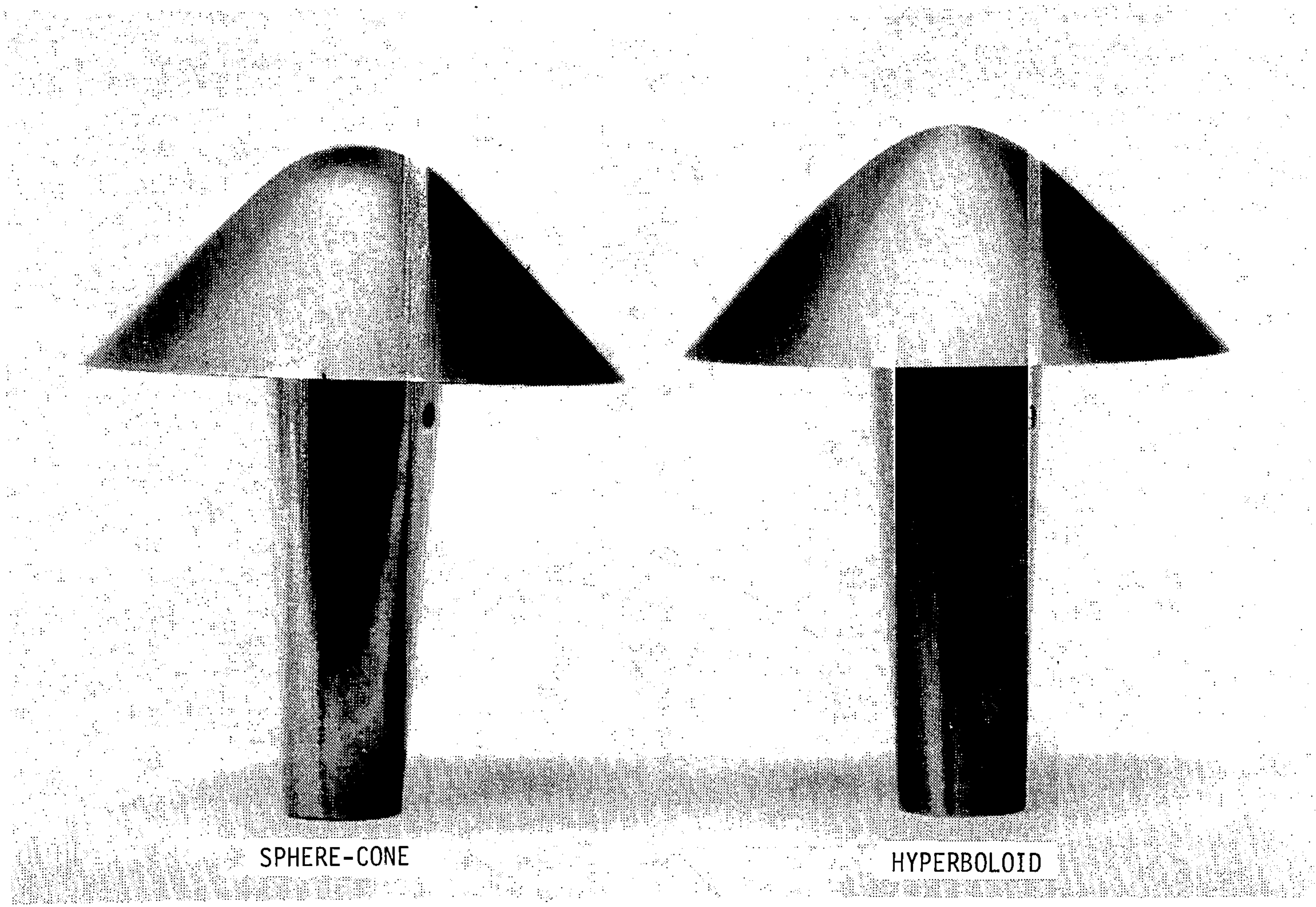

L-82-208

Figure 5.- Force-test models.

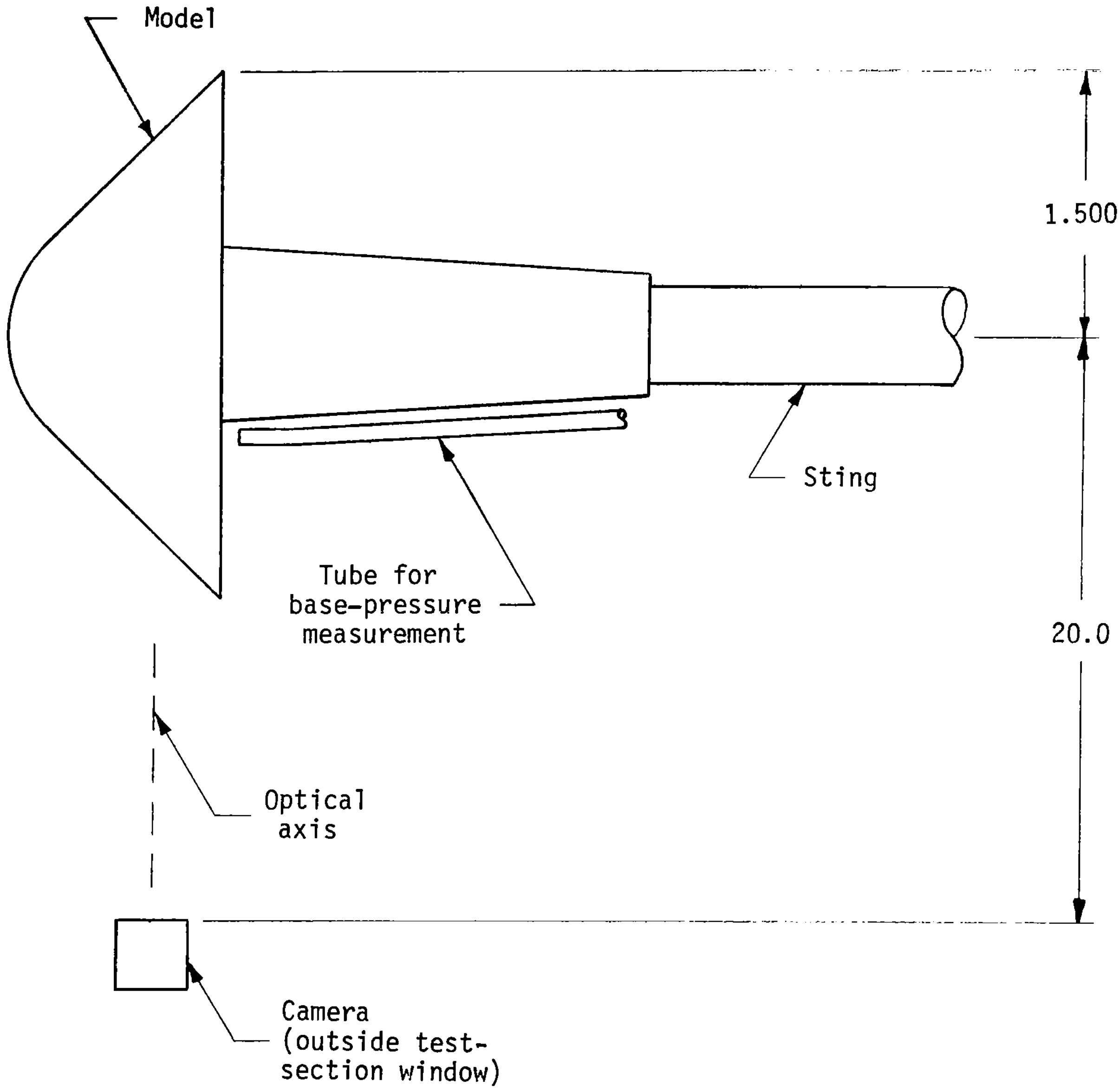

Figure 6.- Sketch of tunnel setup. (All dimensions in inches.)

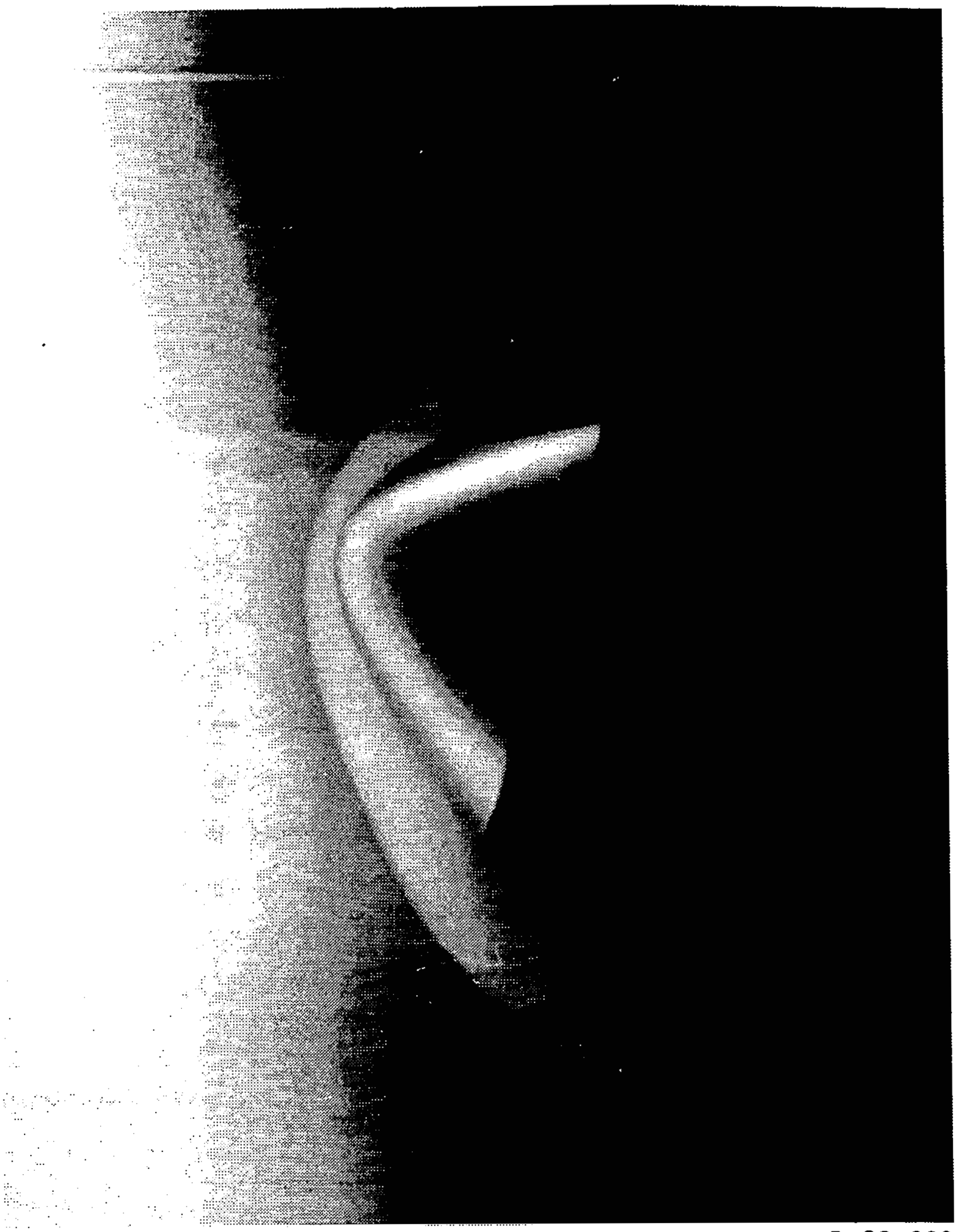

L-82-209

Figure 7.- Example of electron-beam photograph.

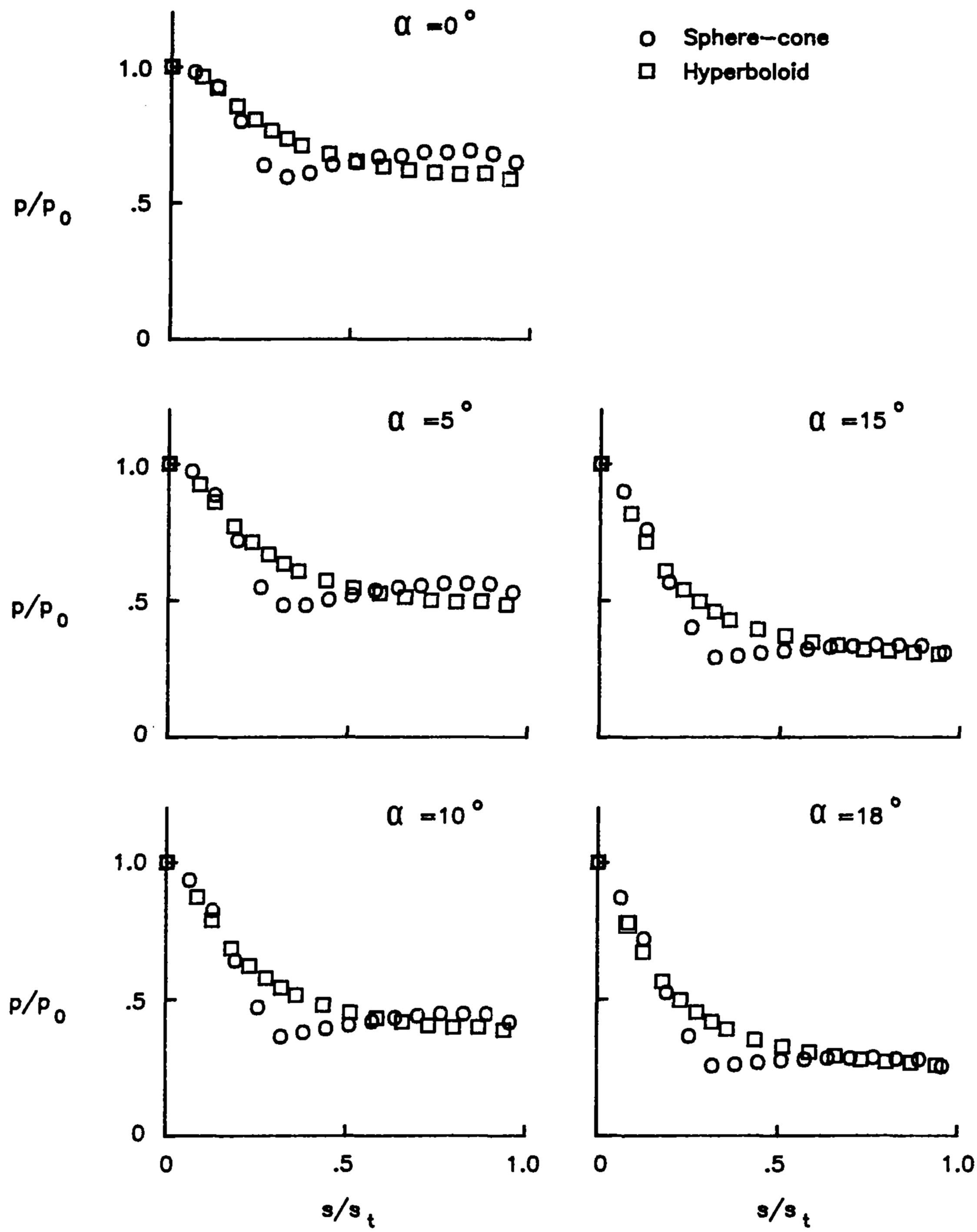

(a) $\phi = 0°$.

Figure 8.- Measured pressures on the sphere-cone and hyperboloid.

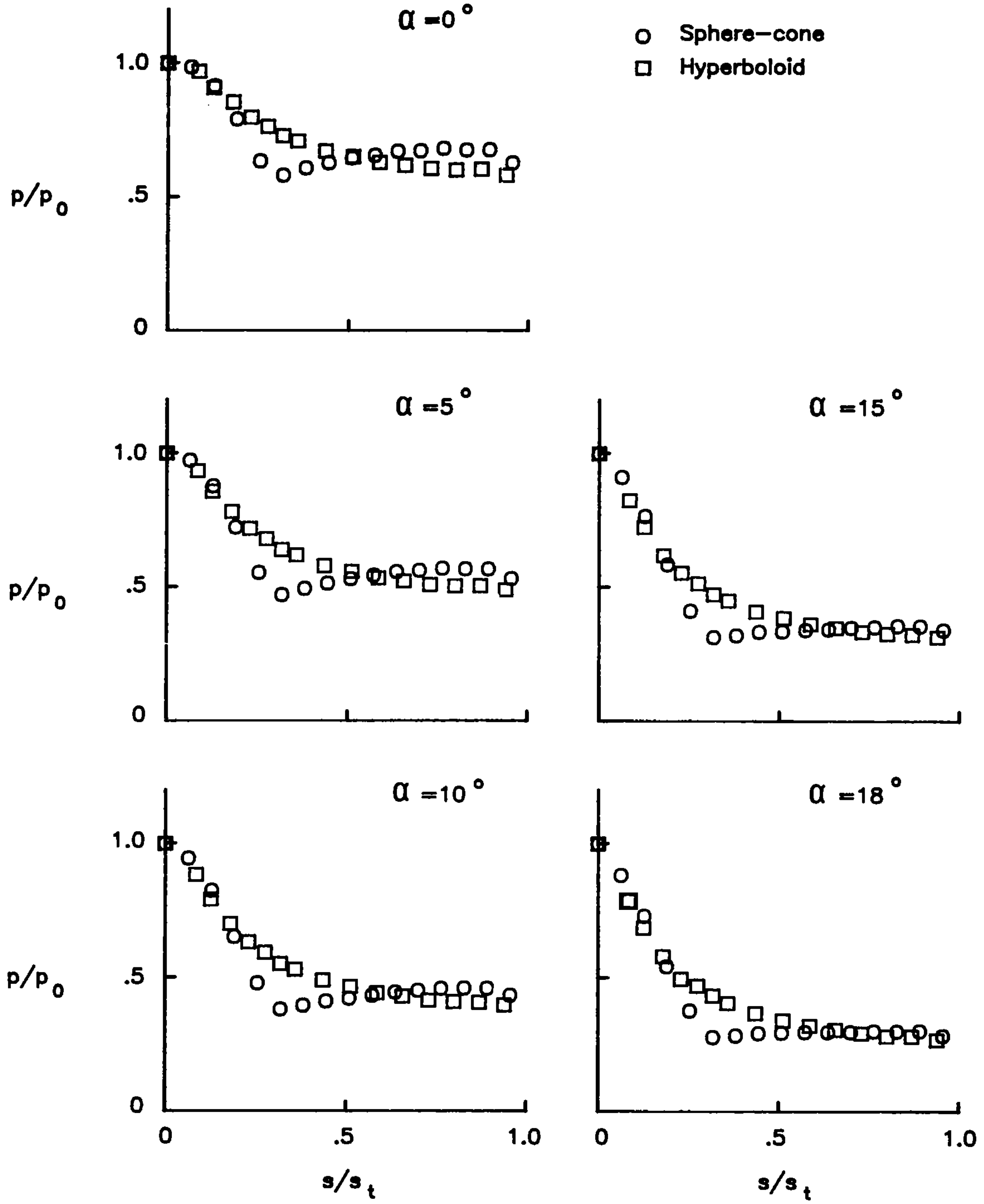

(b) $\phi = 22.5°$.

Figure 8.- Continued.

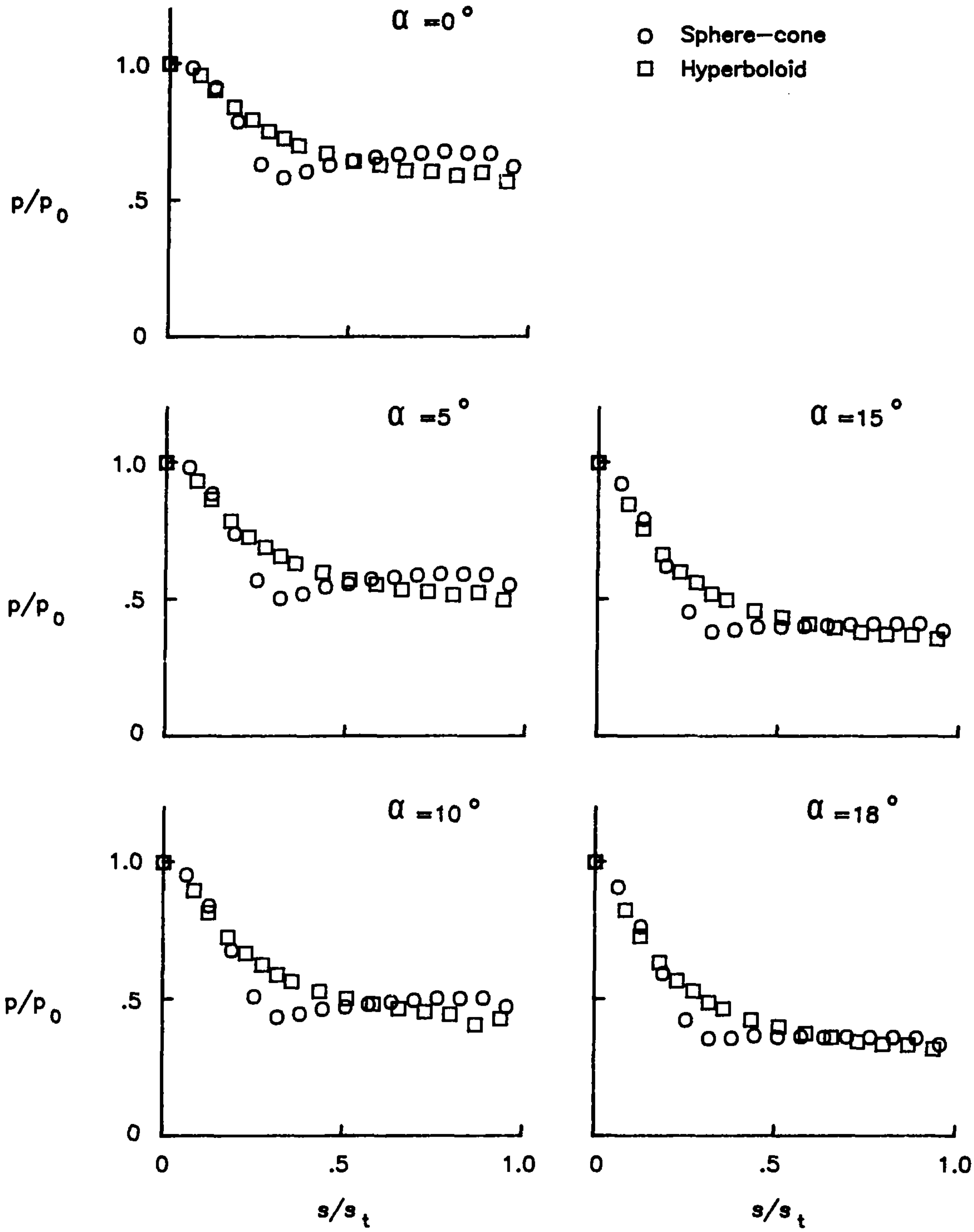

(c) ϕ = 45°.

Figure 8.- Continued.

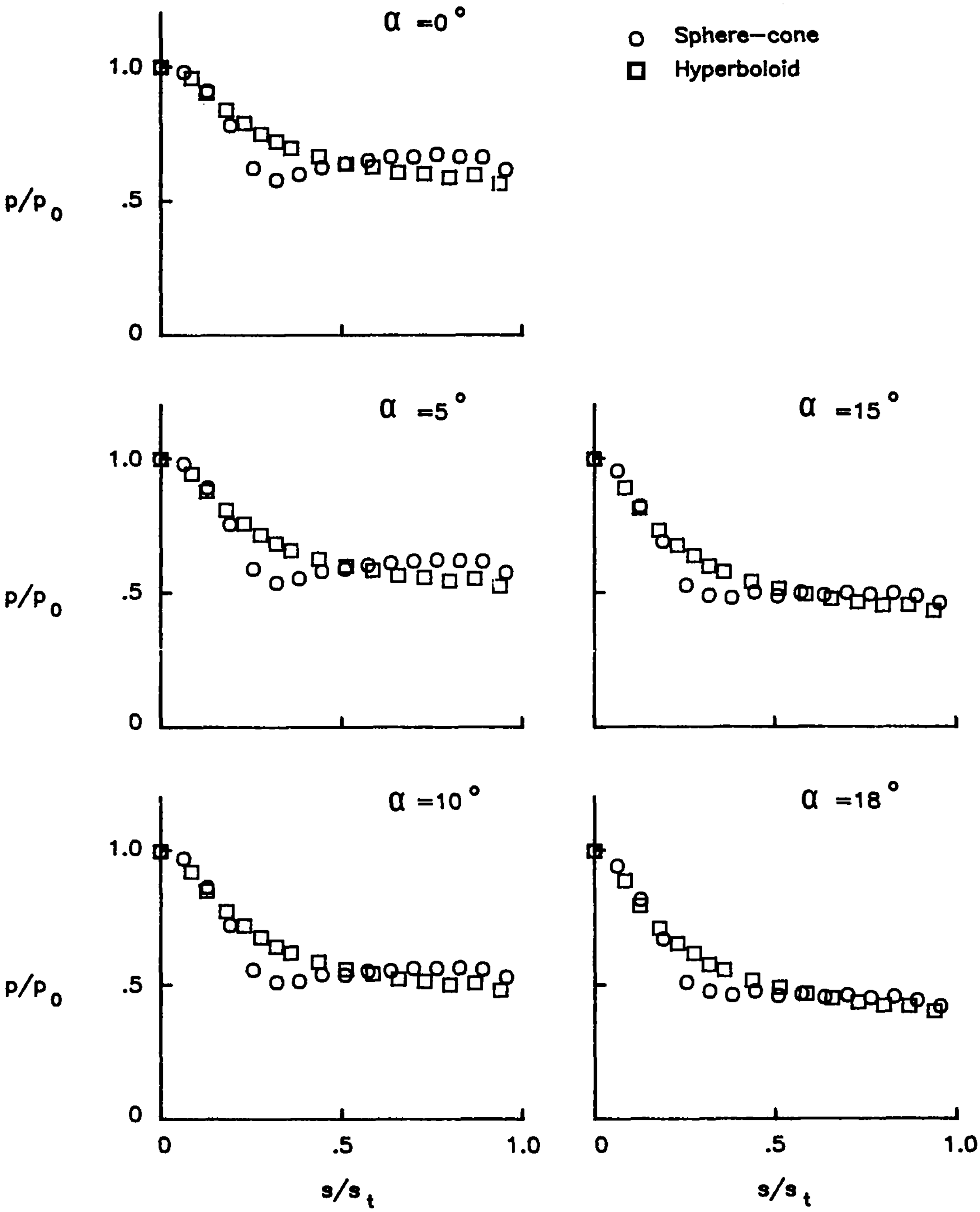

(d) $\phi = 67.5°$.

Figure 8.- Continued.

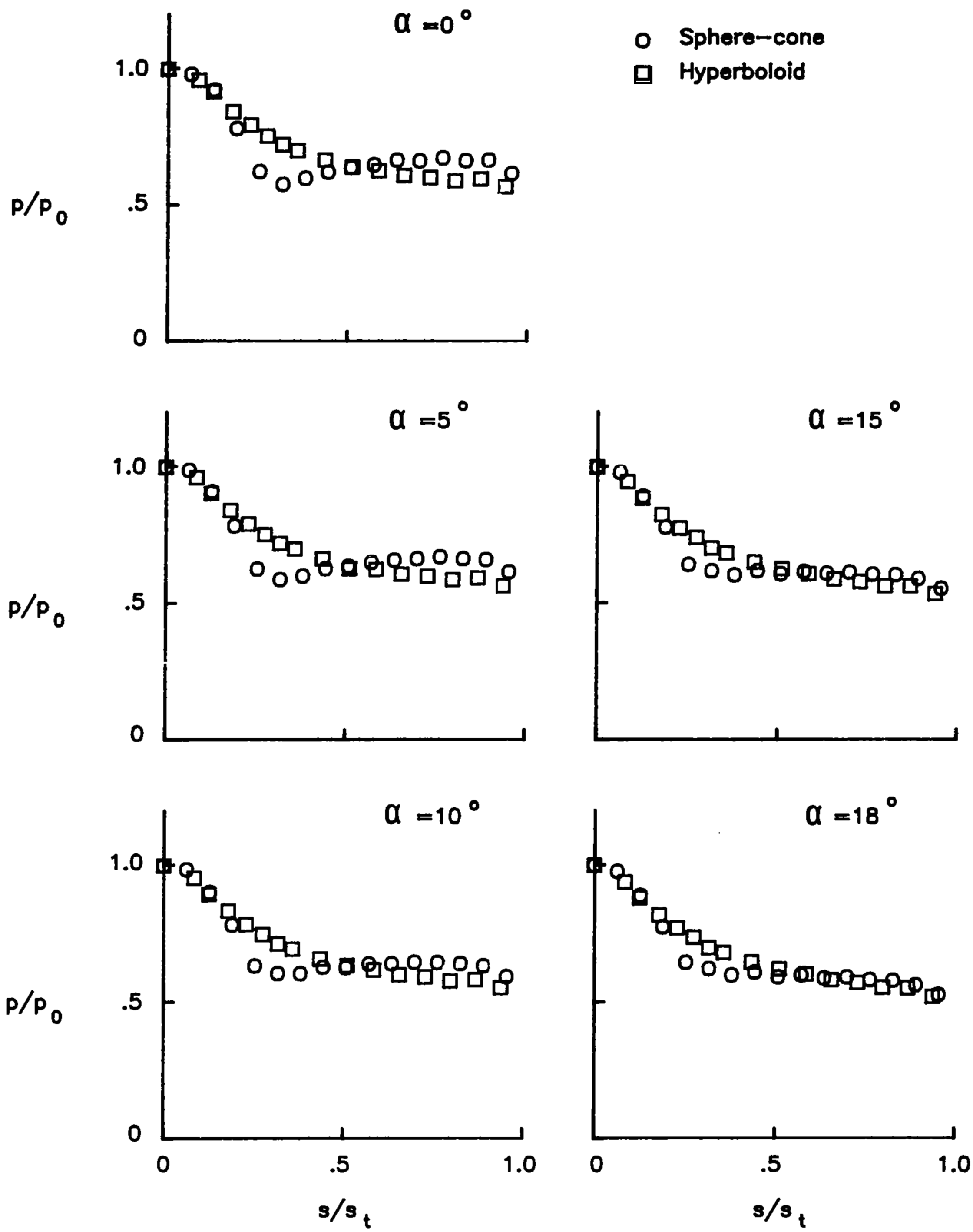

(e) ϕ = 90°.

Figure 8.- Continued.

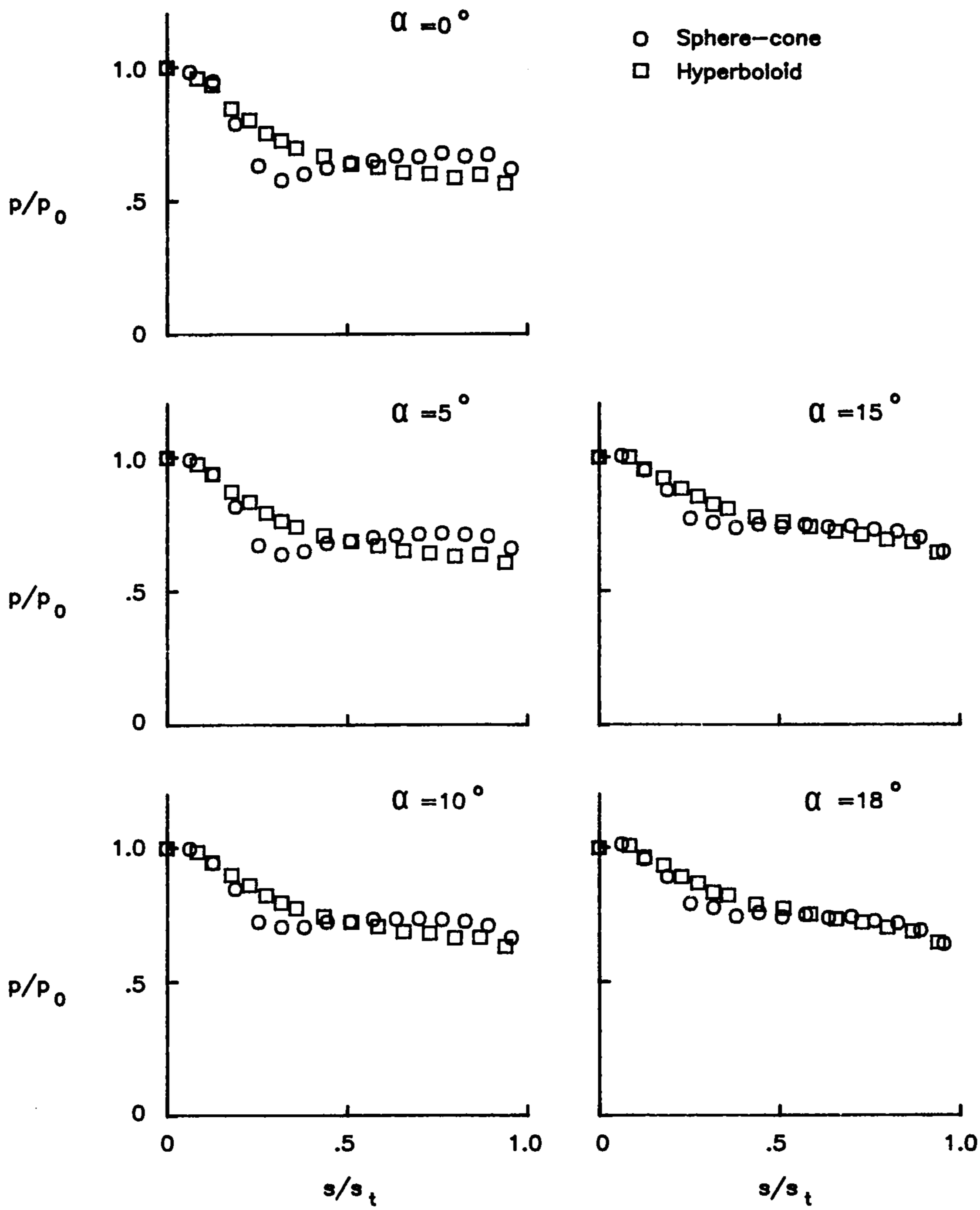

(f) ϕ = 112.5°.

Figure 8.- Continued.

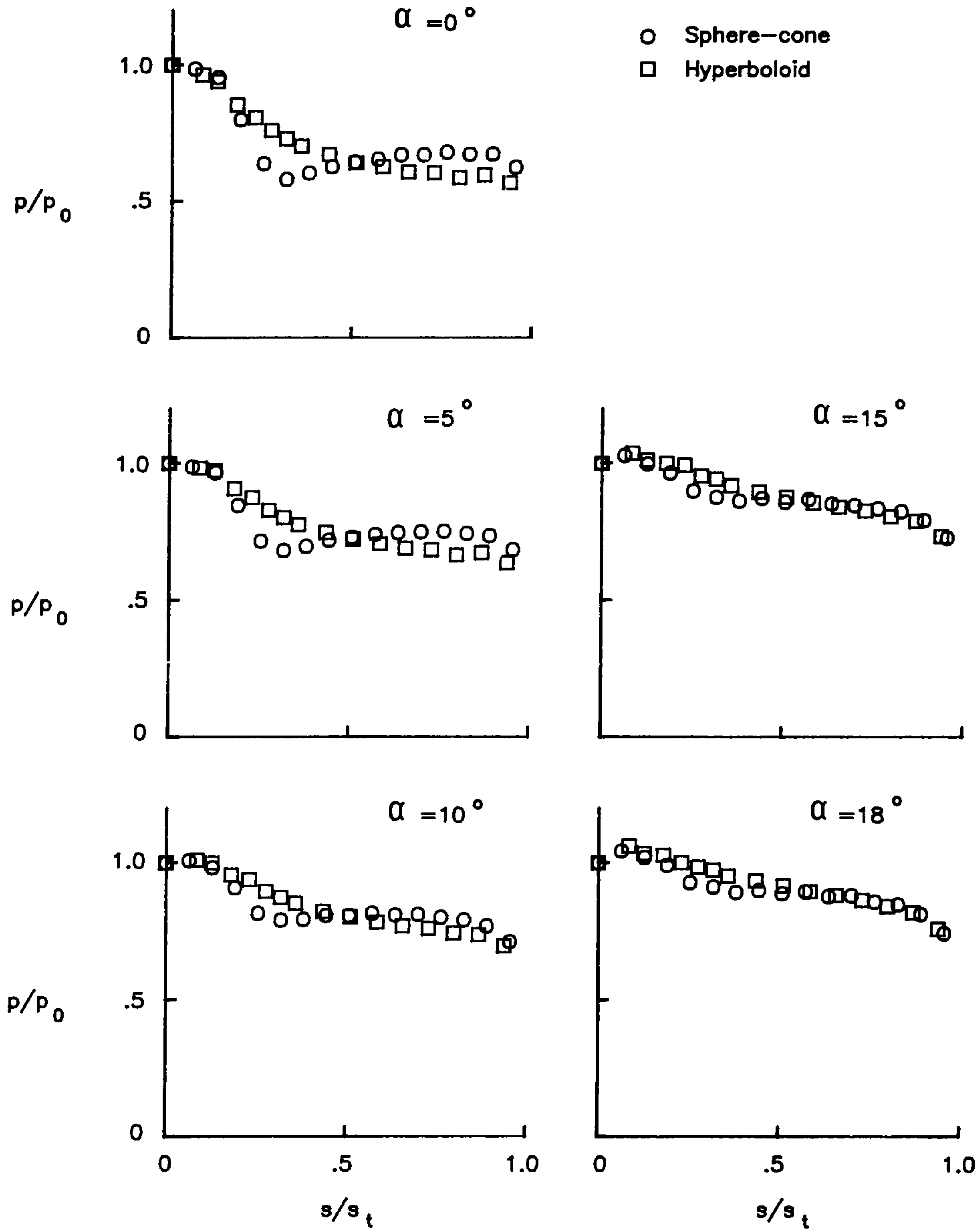

(g) ϕ = 135°.

Figure 8.- Continued.

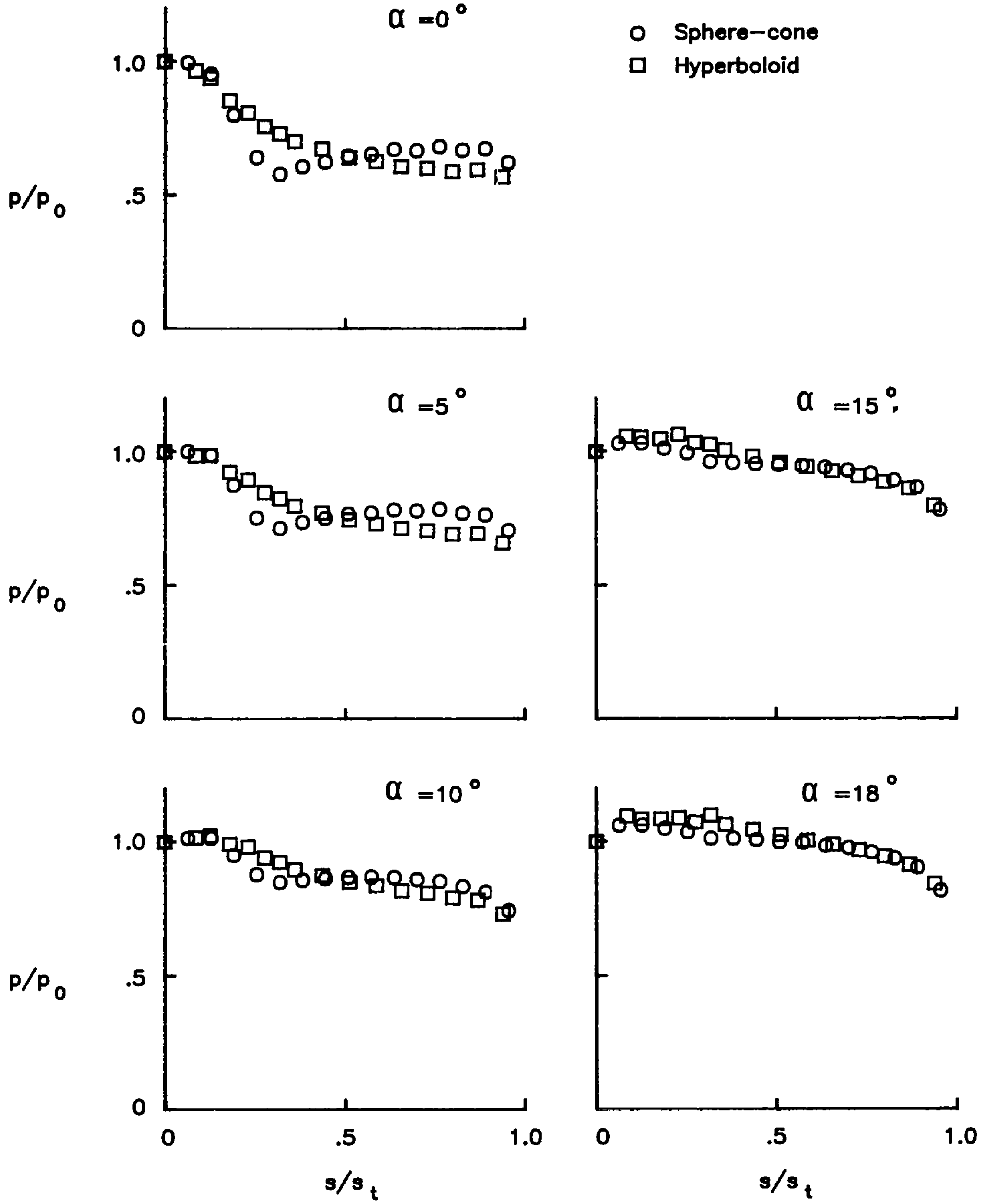

(h) ϕ = 157.5°.

Figure 8.- Continued.

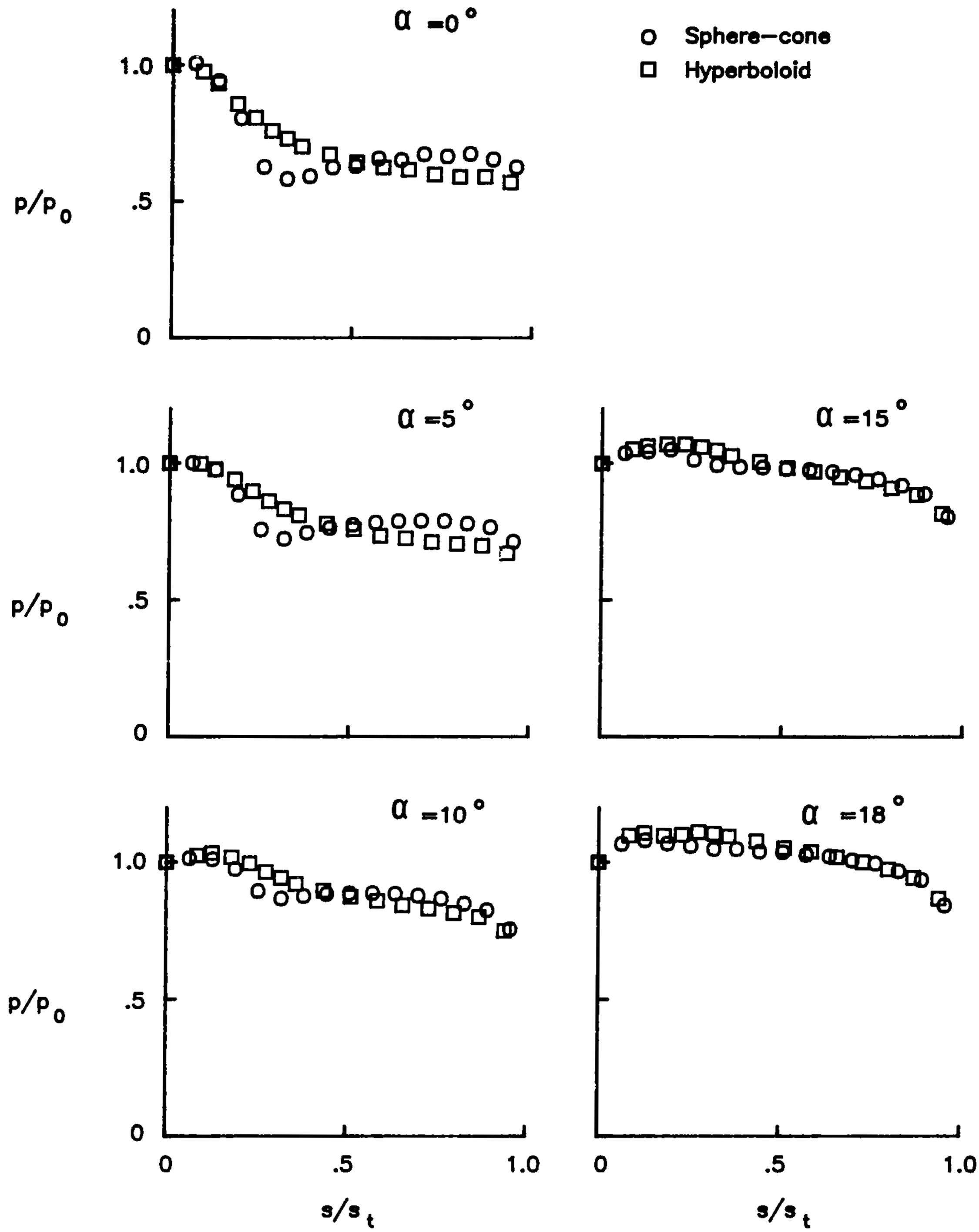

(i) $\phi = 180°$.

Figure 8.- Concluded.

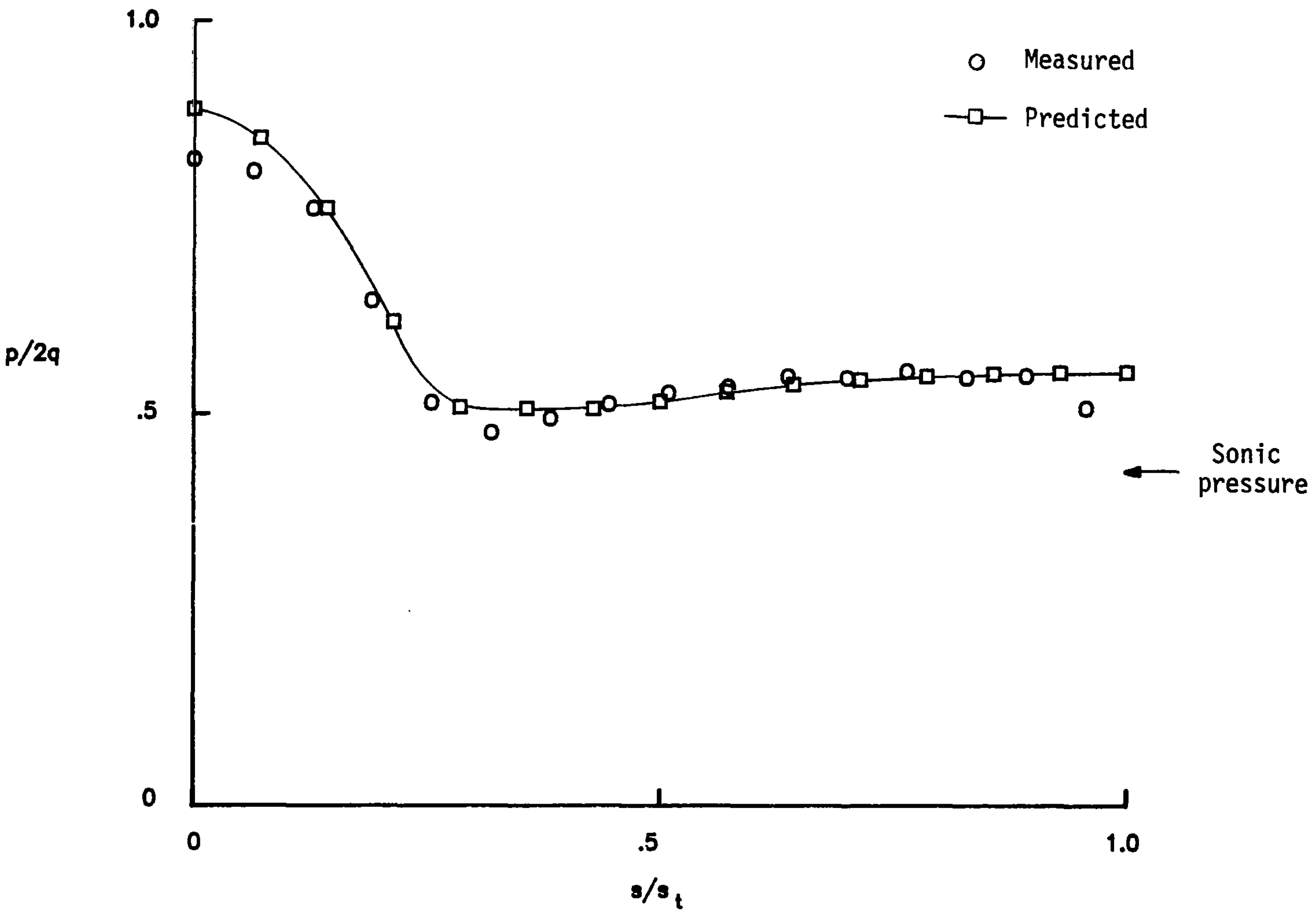

(a) $\alpha = 0°$.

Figure 9.- Measured and predicted pressures on the sphere-cone.

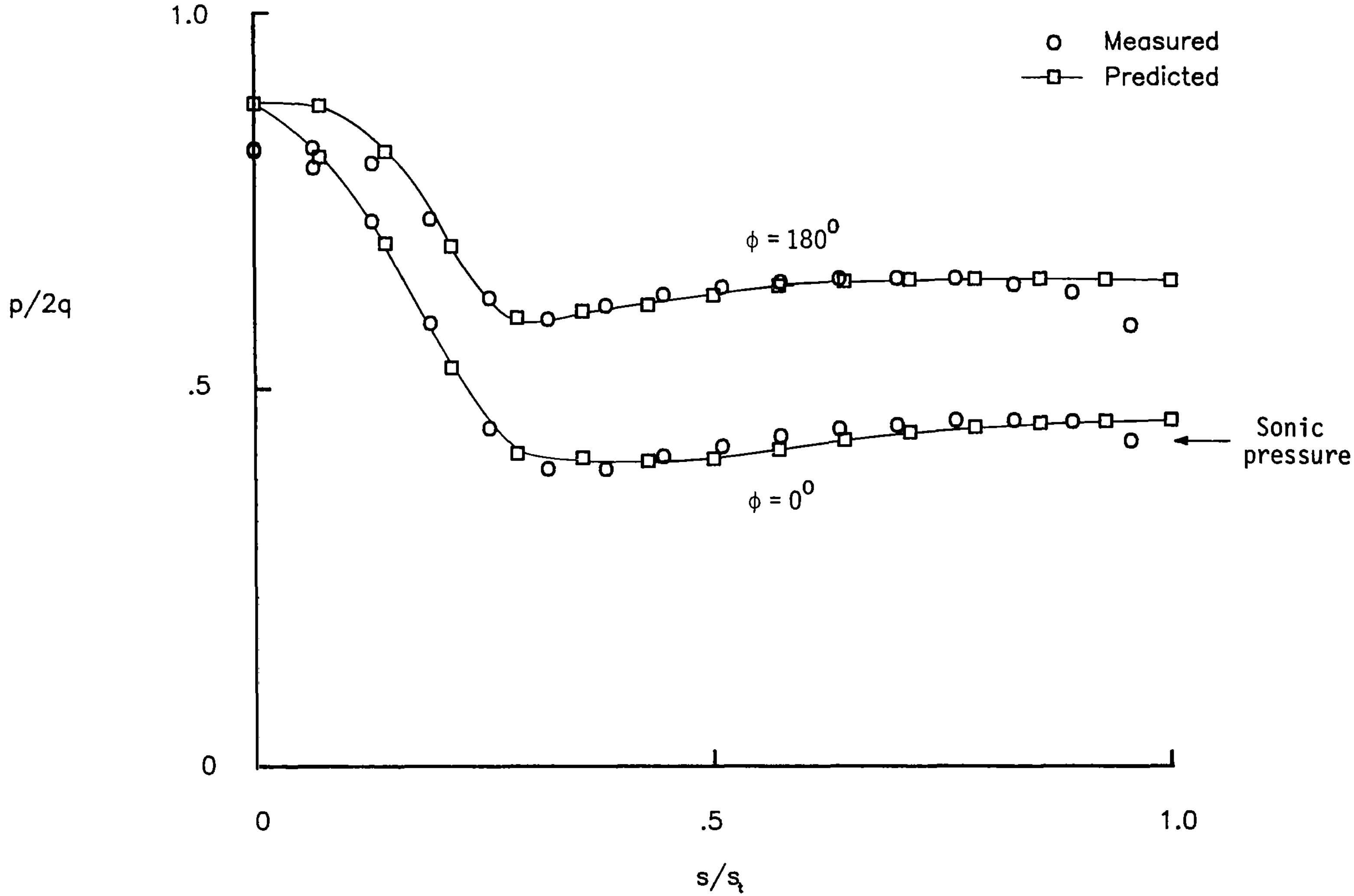

(b) $\alpha = 5°$.

Figure 9.- Continued.

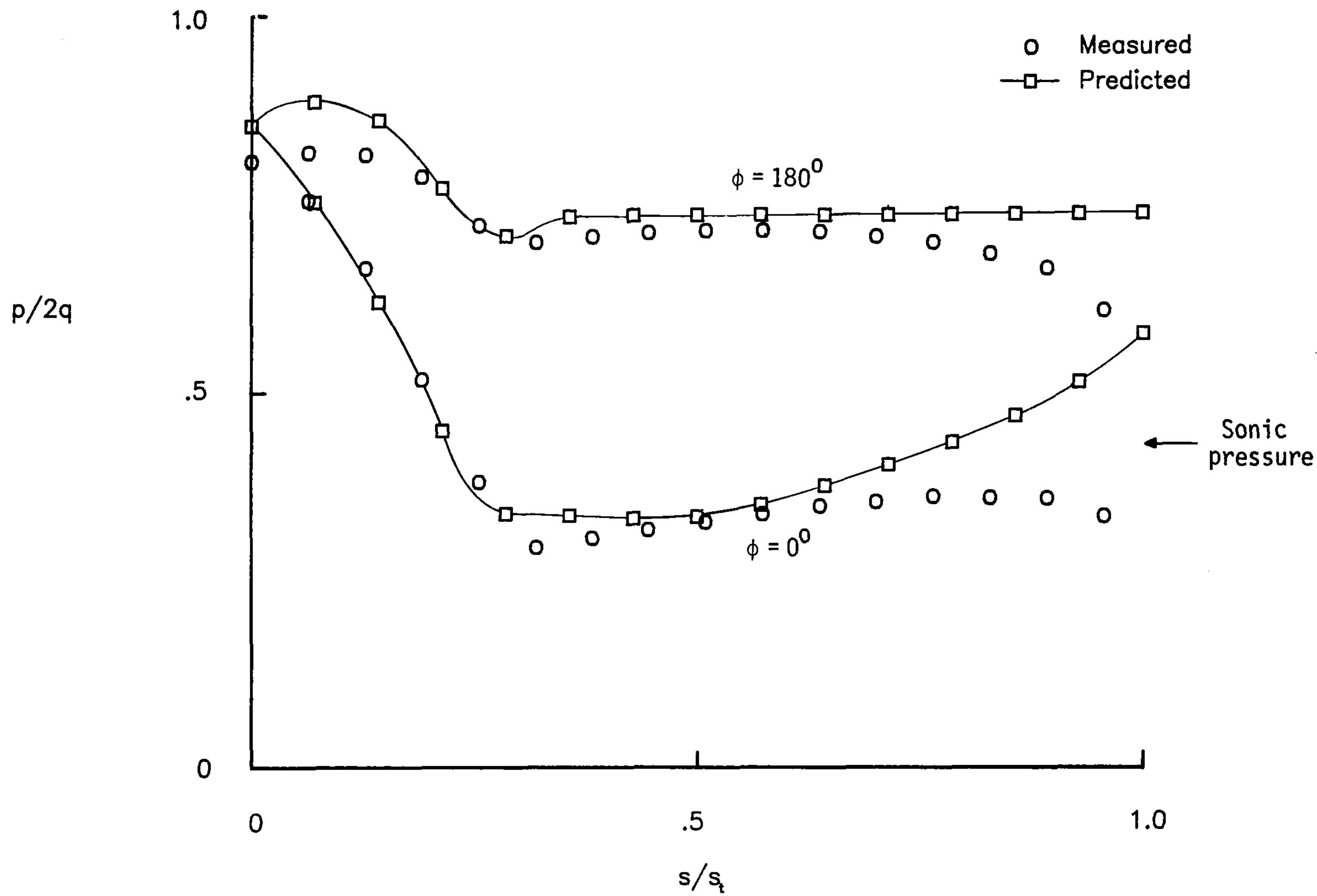

(c) $\alpha = 10°$.

Figure 9.- Concluded.

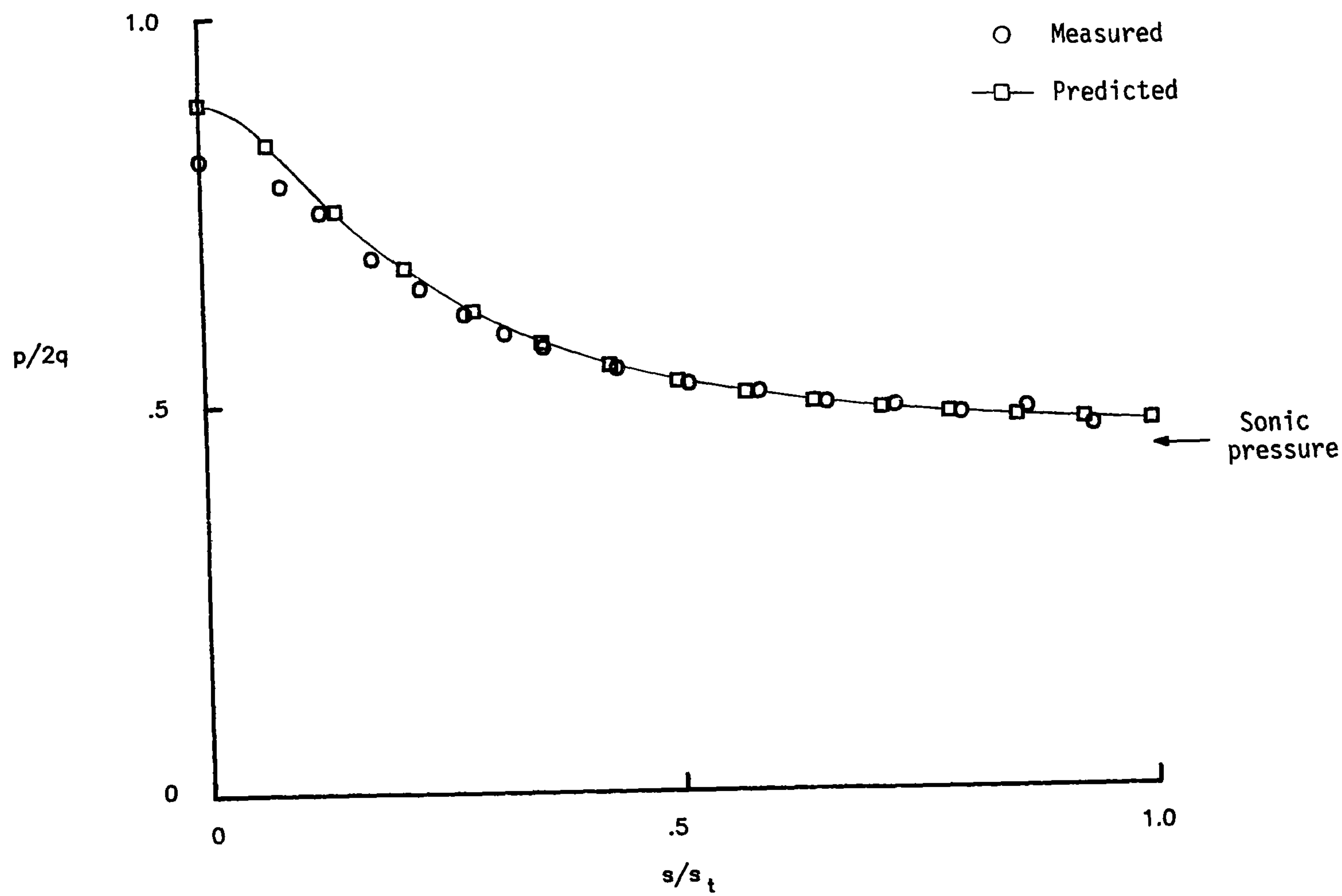

(a) $\alpha = 0°$.

Figure 10.- Measured and predicted pressures on the hyperboloid.

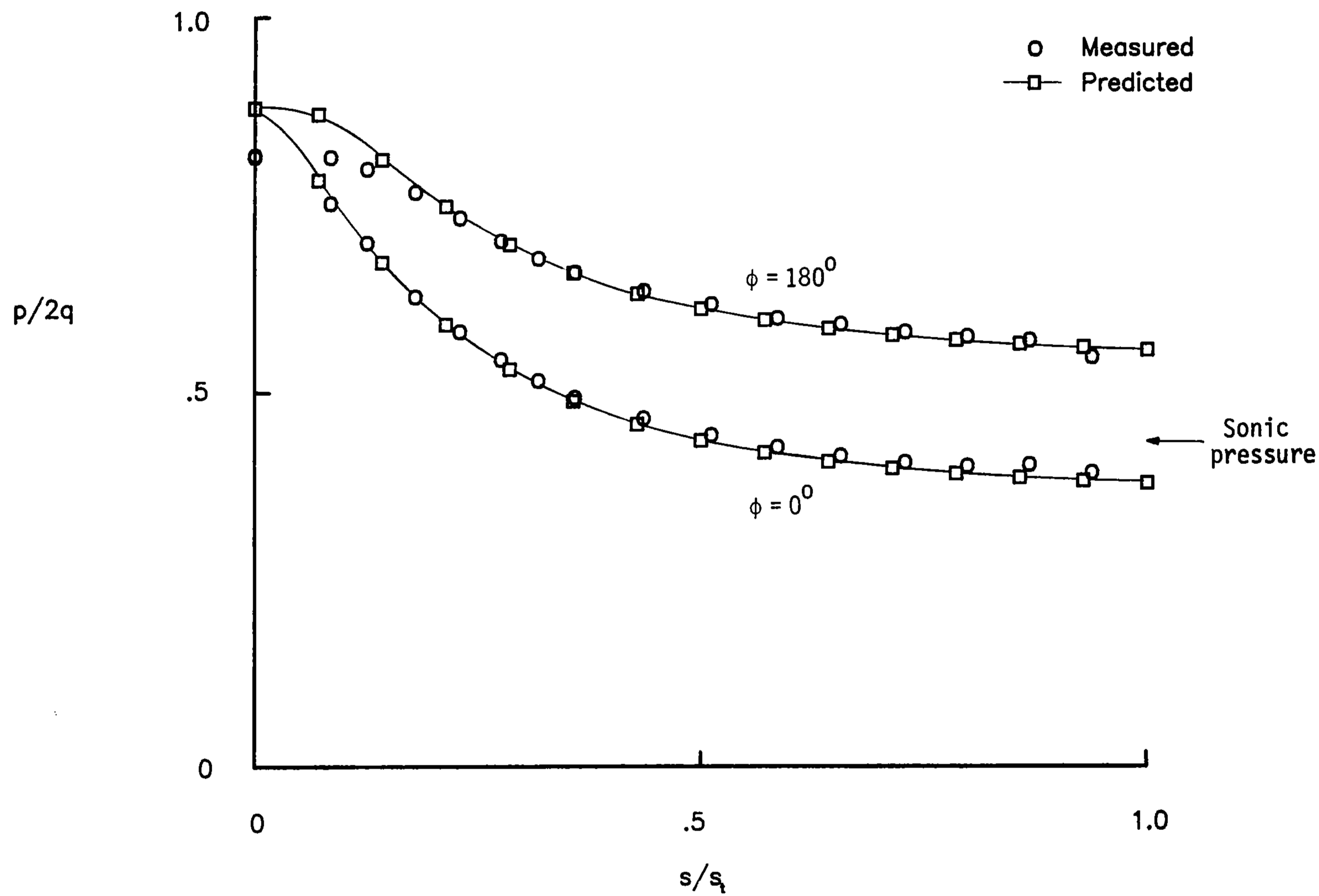

(b) $\alpha = 5°$.

Figure 10.- Continued.

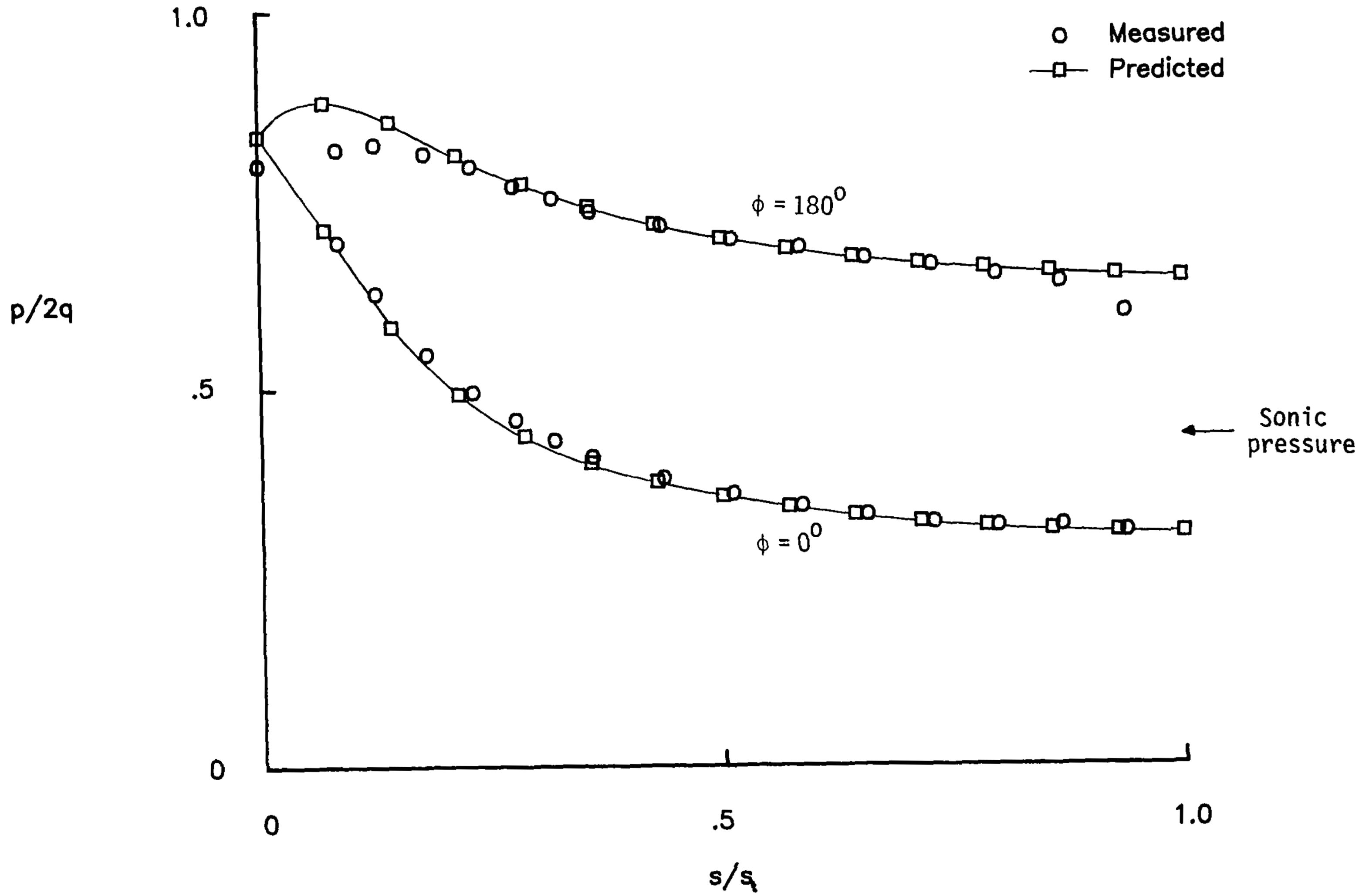

(c) $\alpha = 10°$.

Figure 10.- Continued.

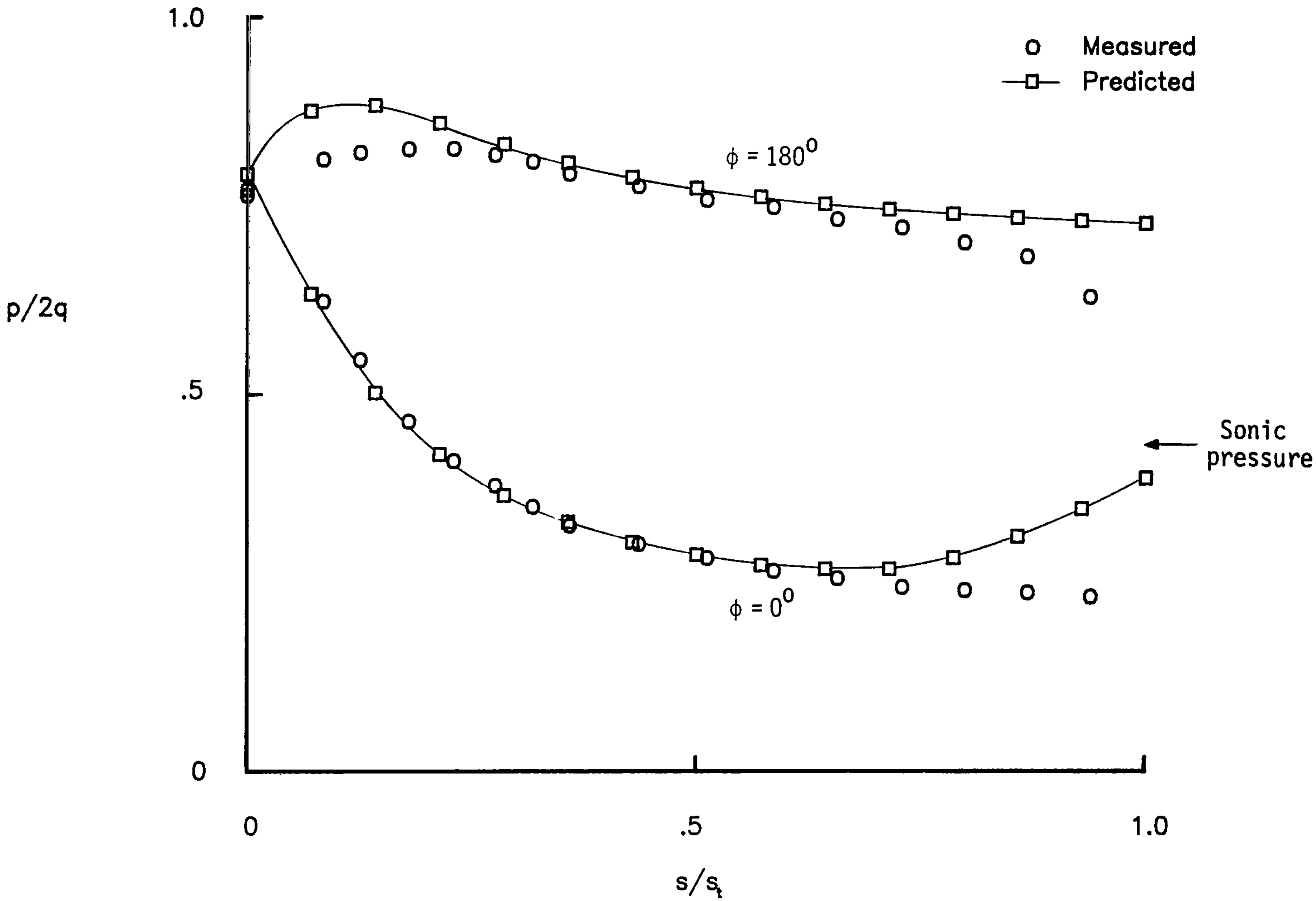

(d) $\alpha = 15°$.

Figure 10.- Concluded.

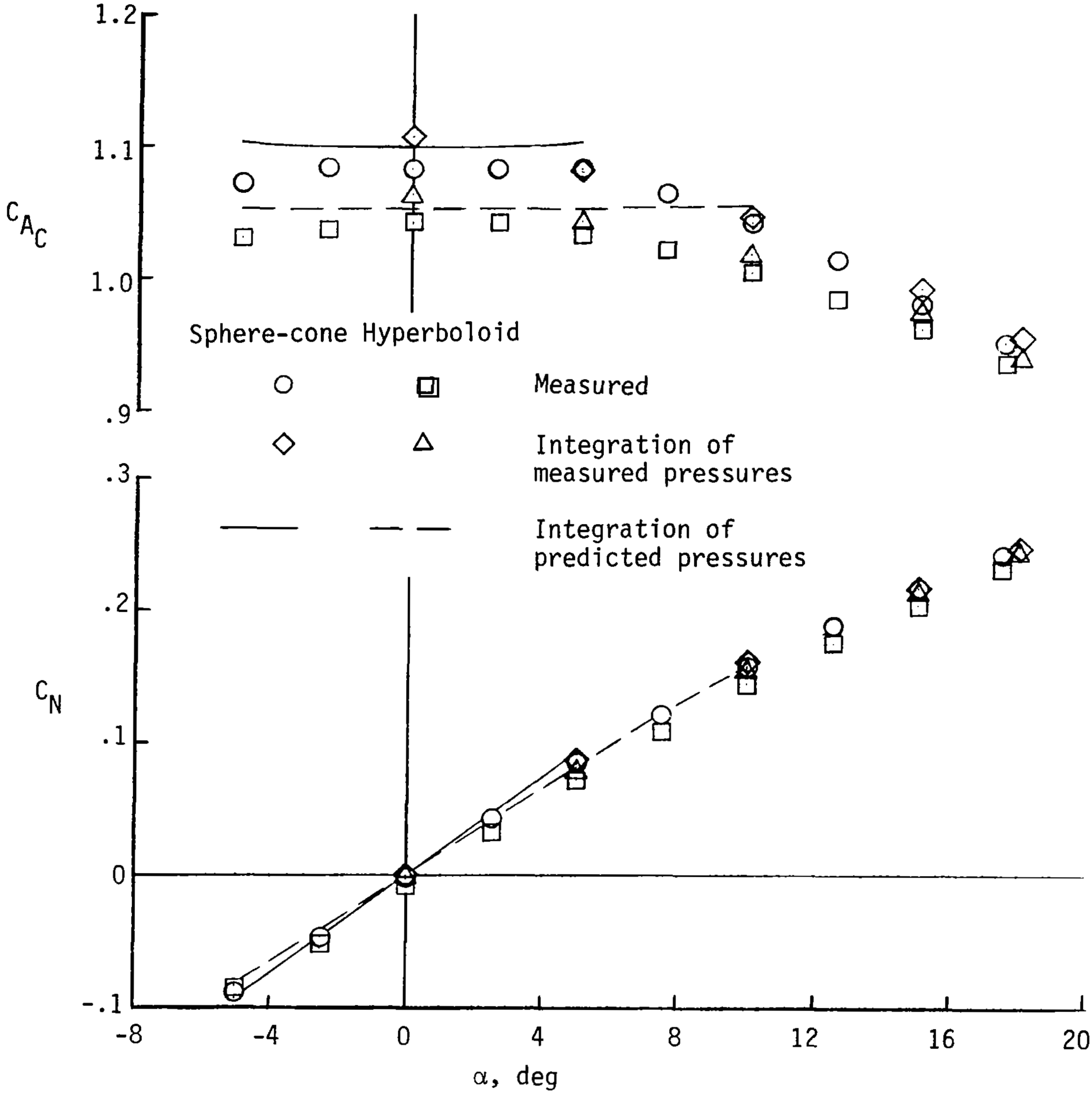

(a) C_{A_C} and C_N versus α.

Figure 11.- Static aerodynamic coefficients.

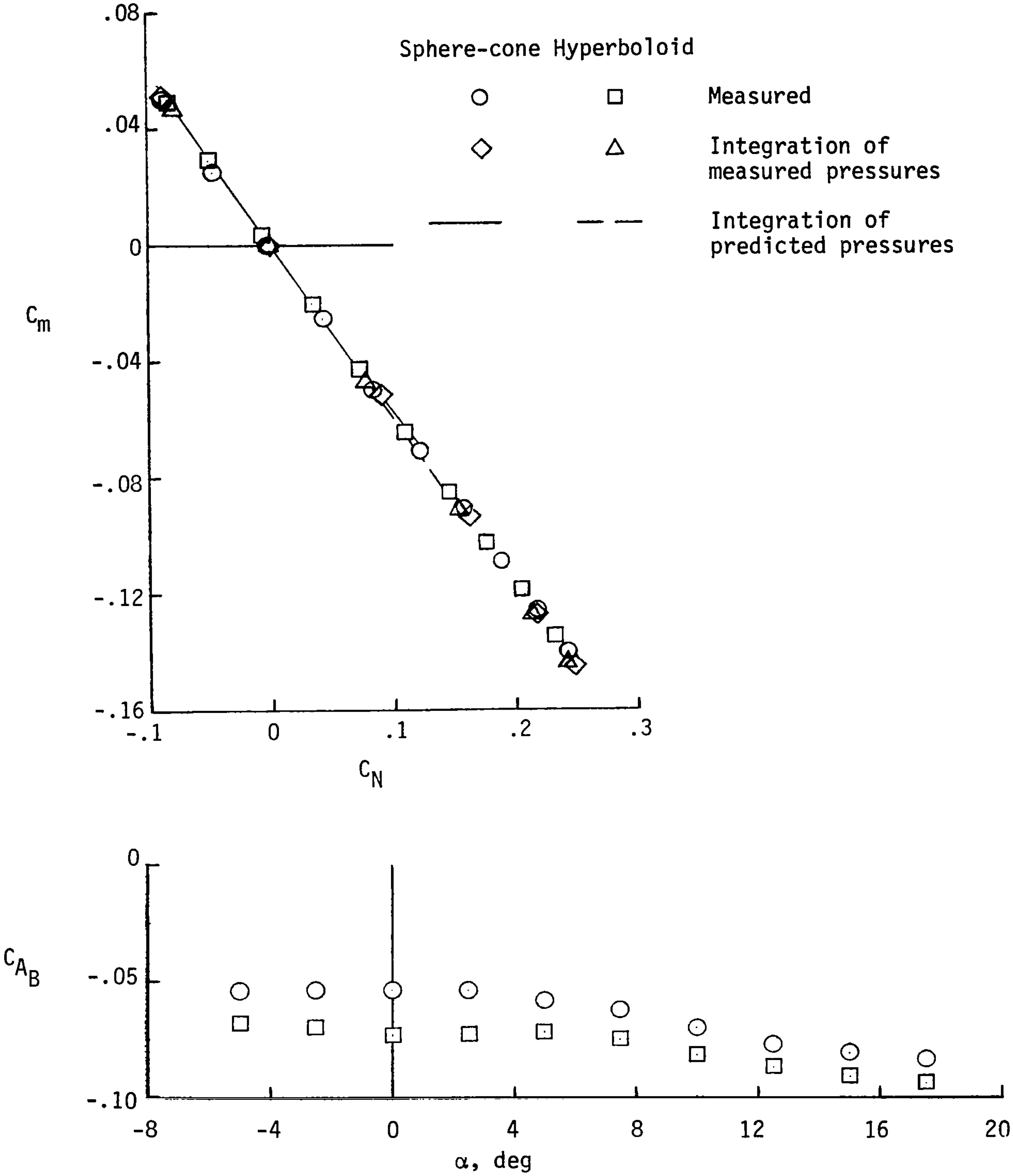

(b) C_m versus C_N and C_{A_B} versus α.

Figure 11.- Continued.

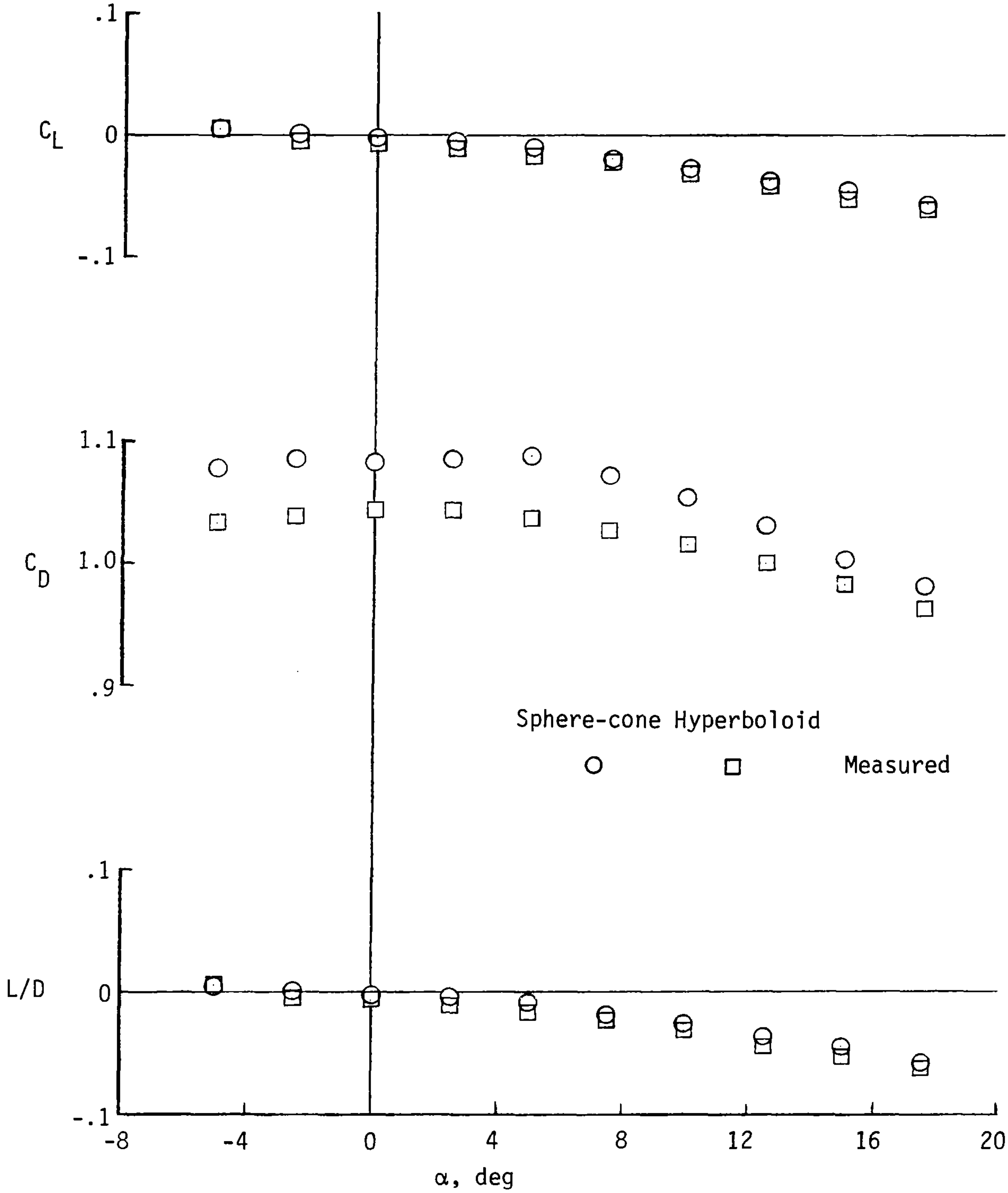

(c) C_L, C_D, and L/D versus α.

Figure 11.- Concluded.

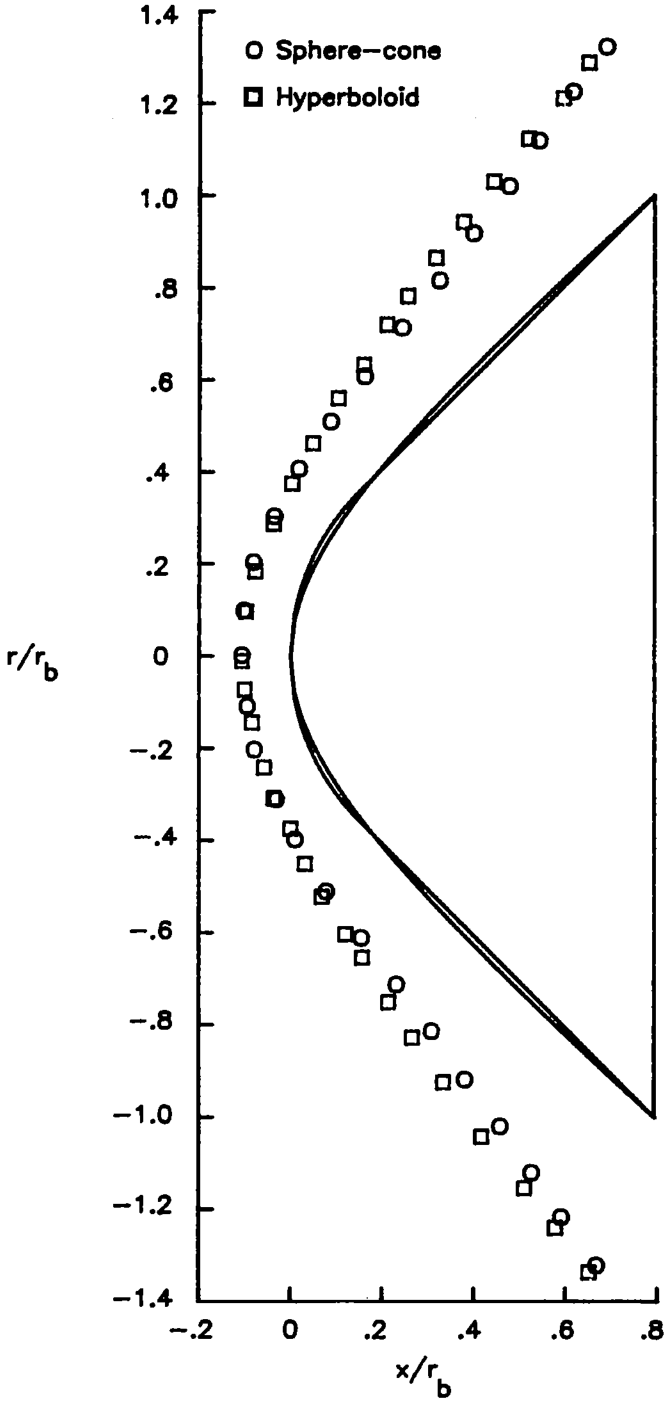

(a) $\alpha = 0°$.

Figure 12.- Measured shock shapes on the sphere-cone and hyperboloid.

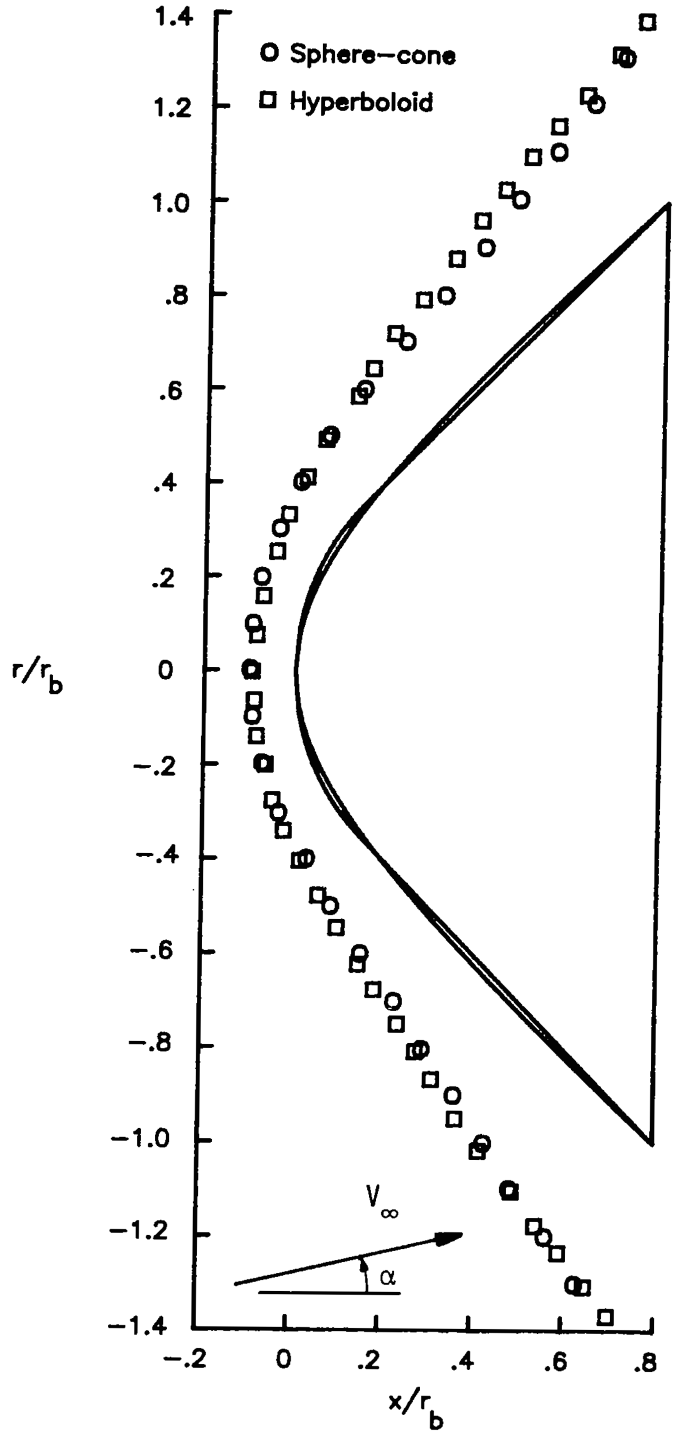

(b) $\alpha = 5°$.

Figure 12.- Continued.

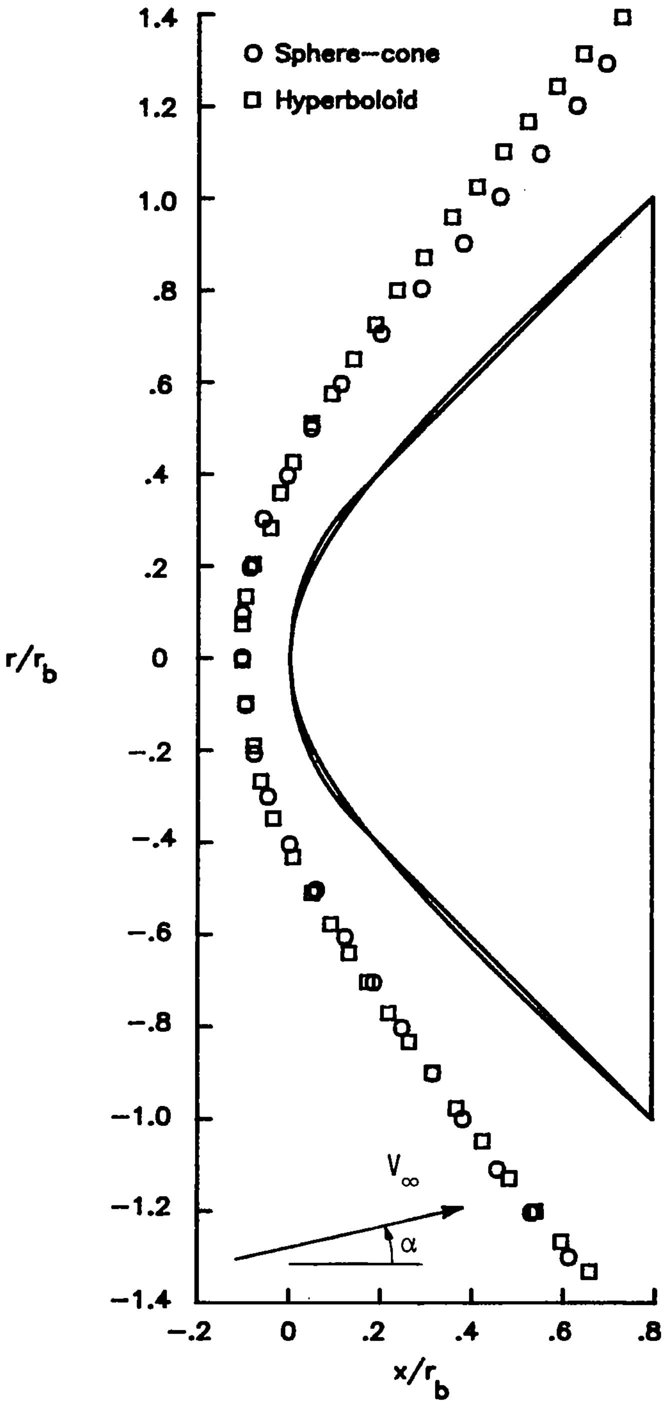

(c) $\alpha = 10°$.

Figure 12.- Continued.

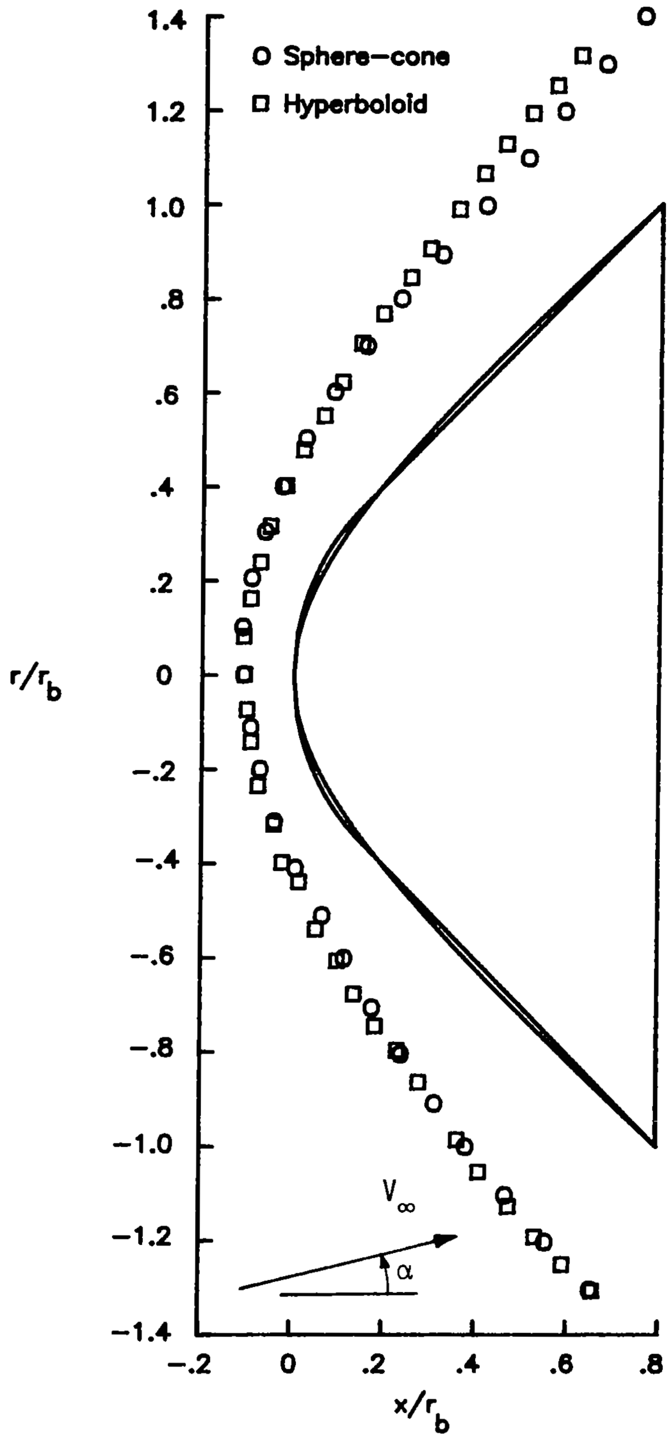

(d) $\alpha = 15°$.

Figure 12.- Continued.

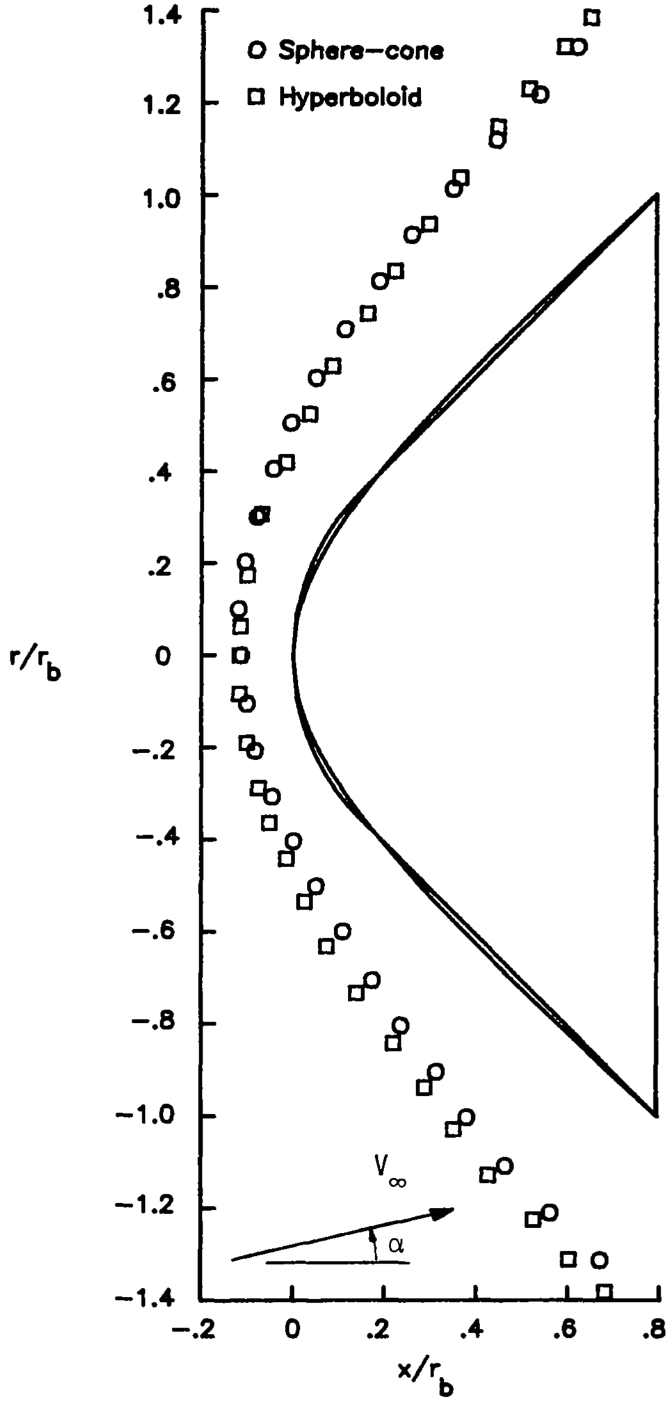

(e) $\alpha = 18°$.

Figure 12.- Concluded.

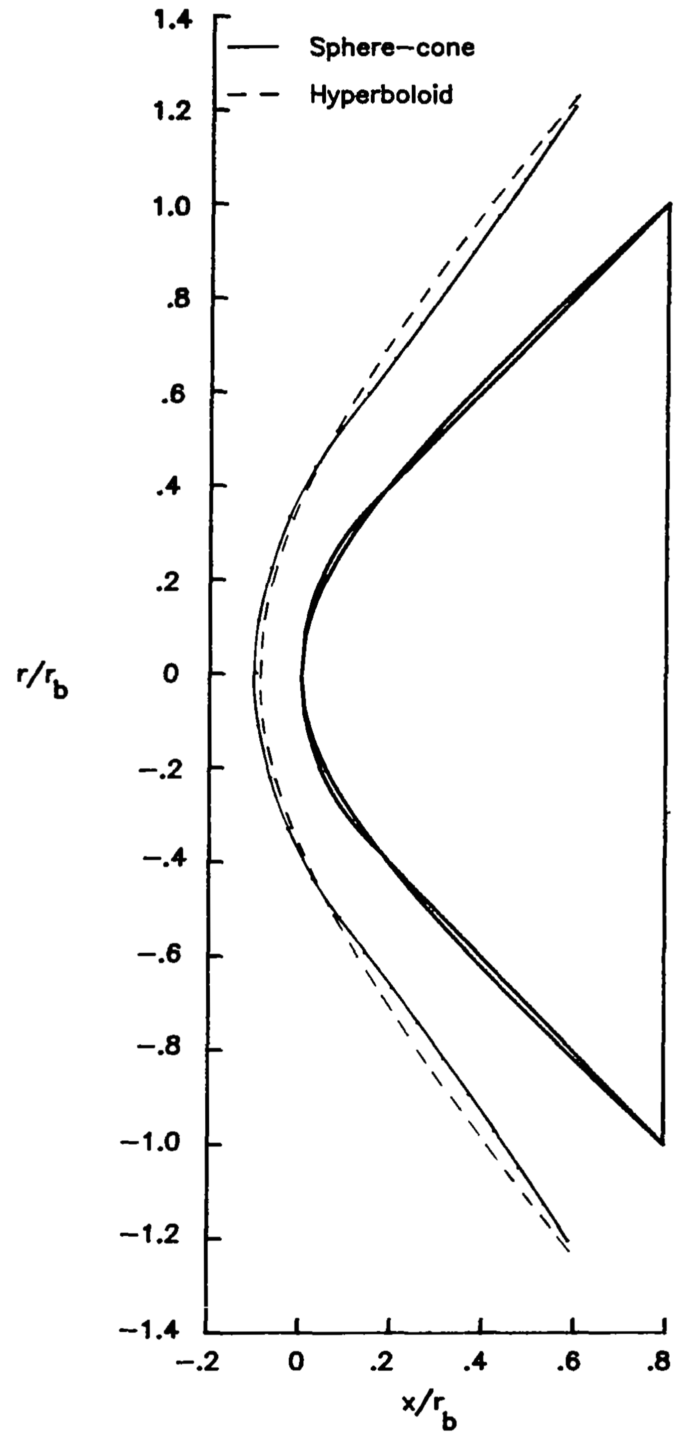

(a) $\alpha = 0°$.

Figure 13.- Predicted shock shapes on the sphere-cone and hyperboloid.

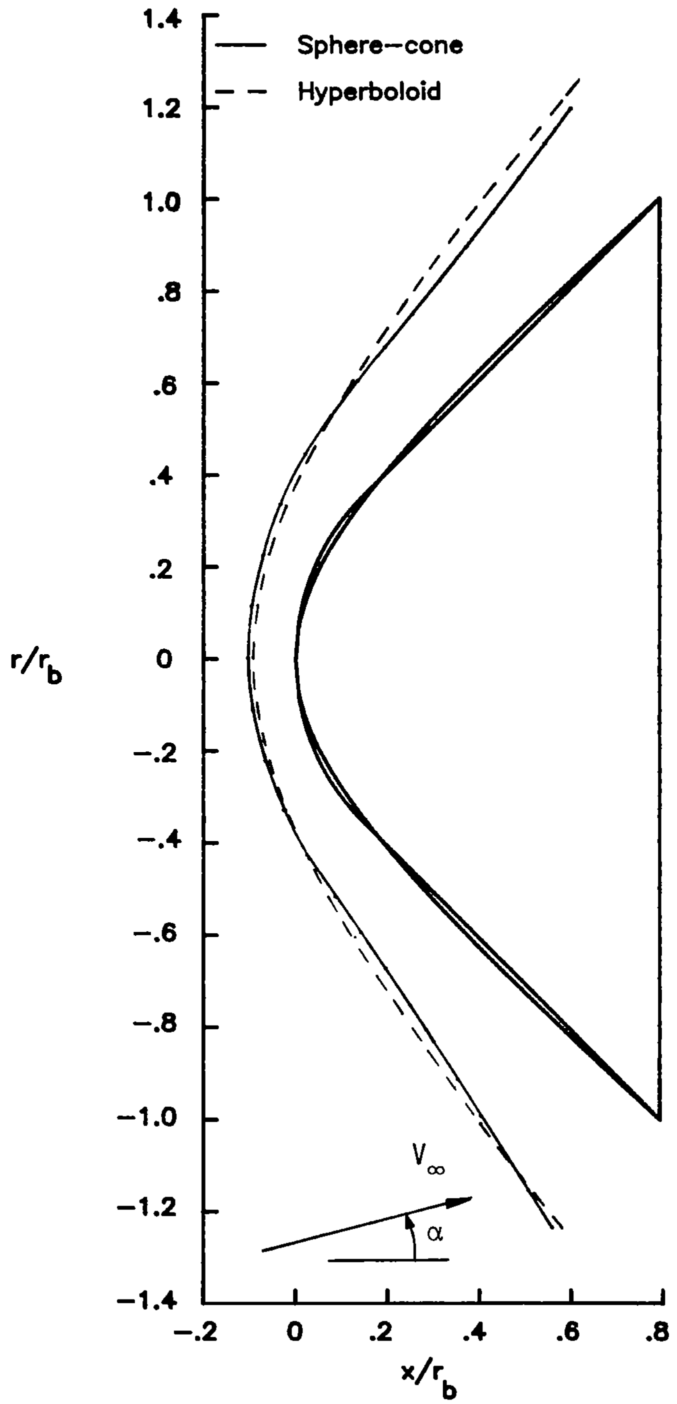

(b) $\alpha = 5°$.

Figure 13.- Concluded.

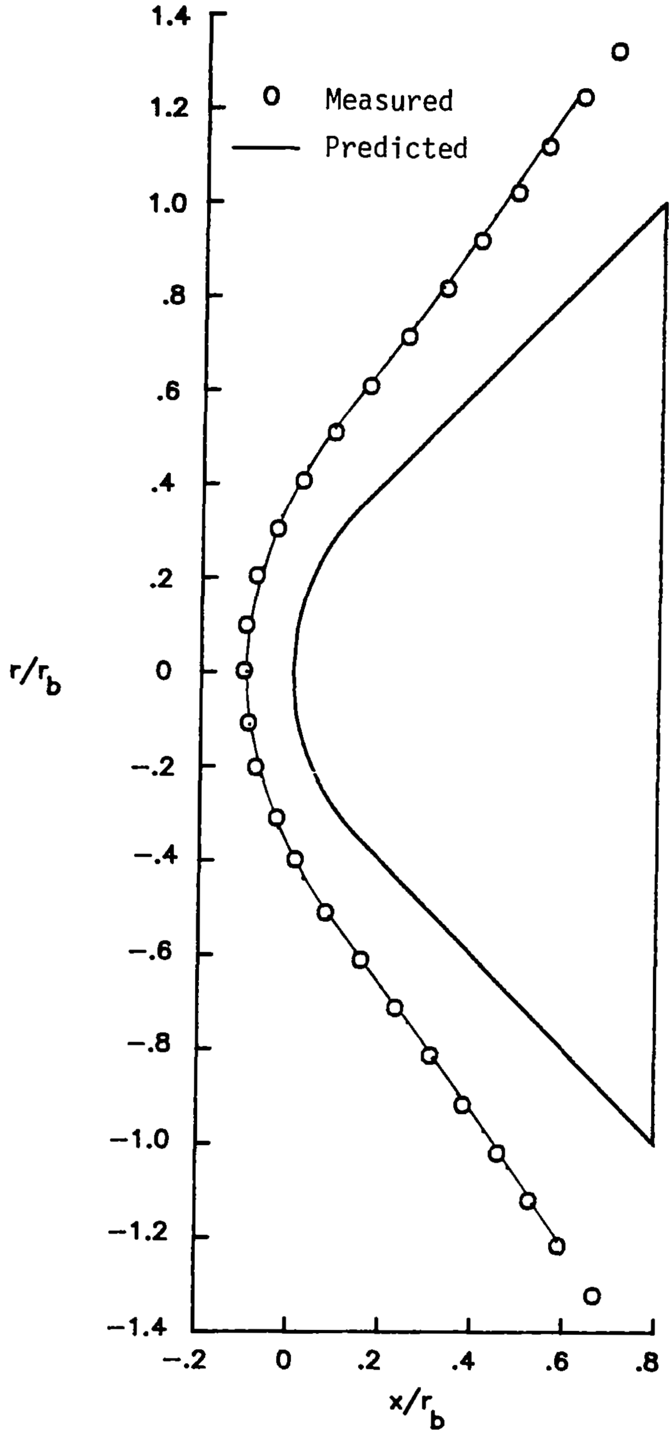

(a) $\alpha = 0°$.

Figure 14.- Measured and predicted shock shapes on the sphere-cone.

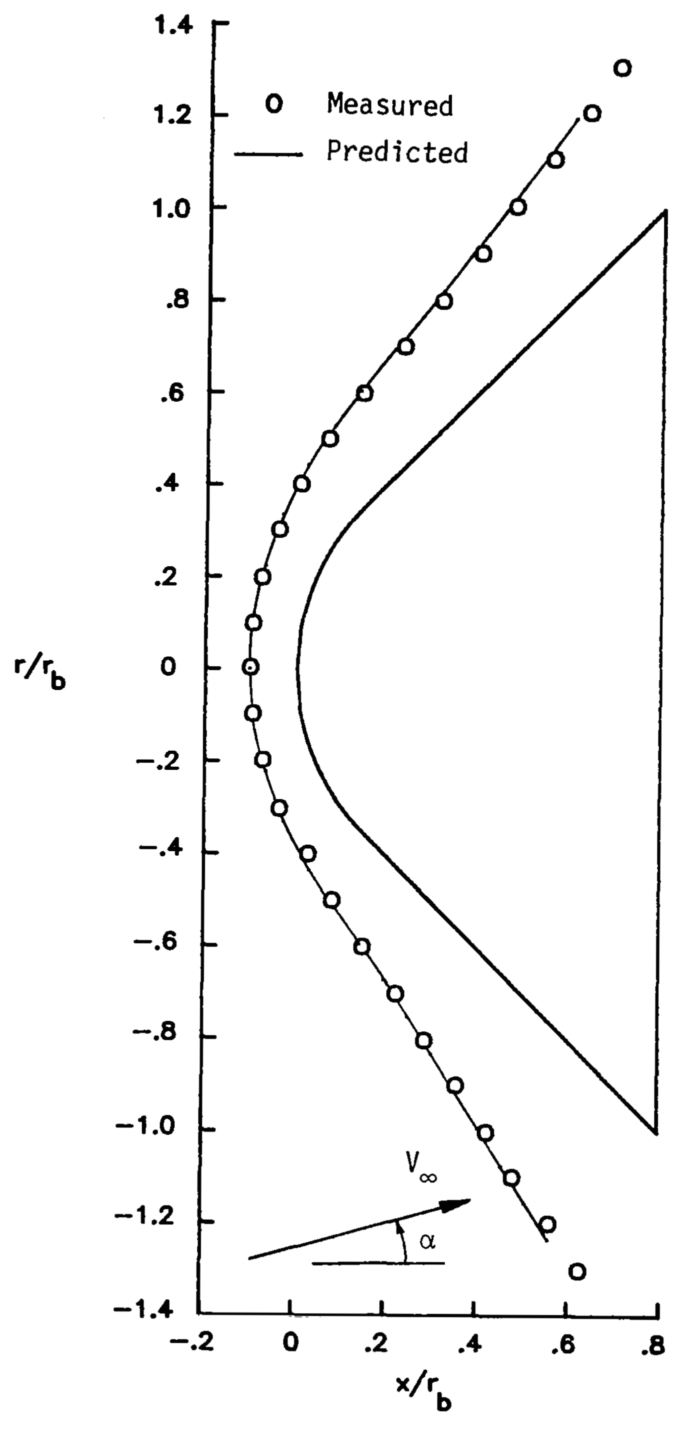

(b) $\alpha = 5°$.

Figure 14.- Continued.

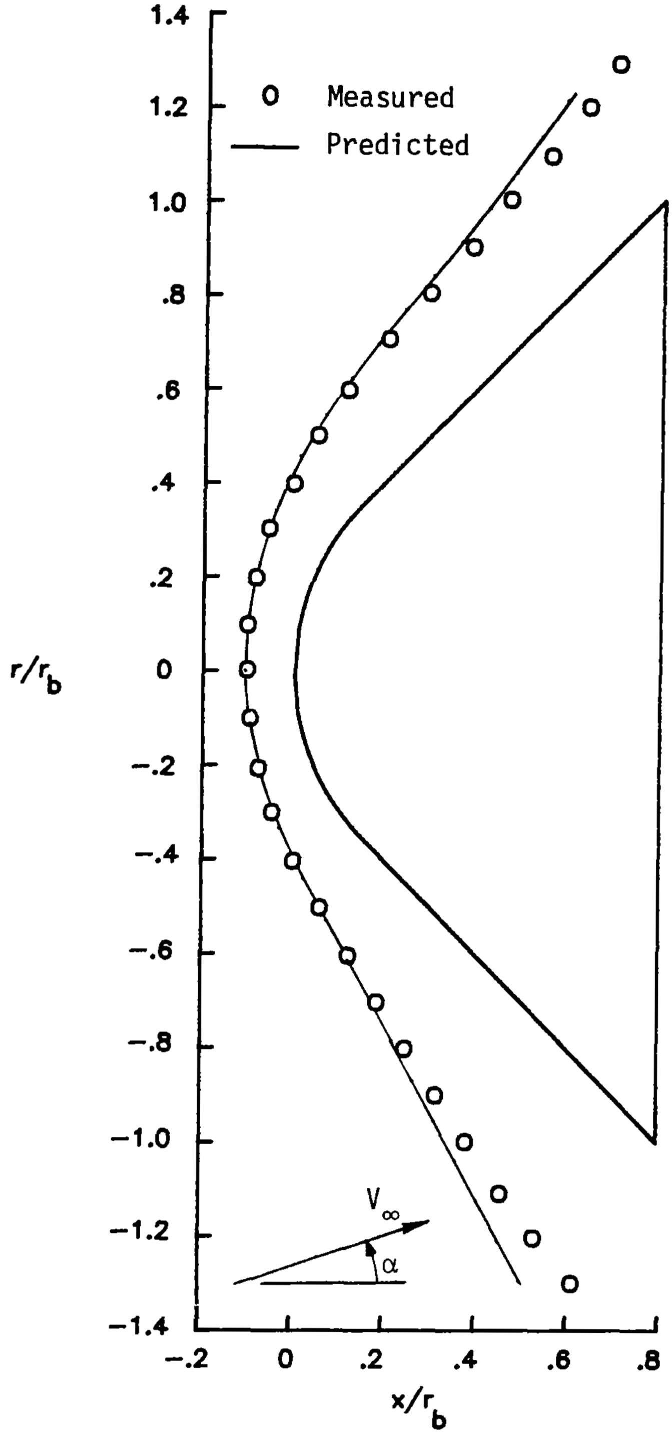

(c) $\alpha = 10°$.

Figure 14.- Concluded.

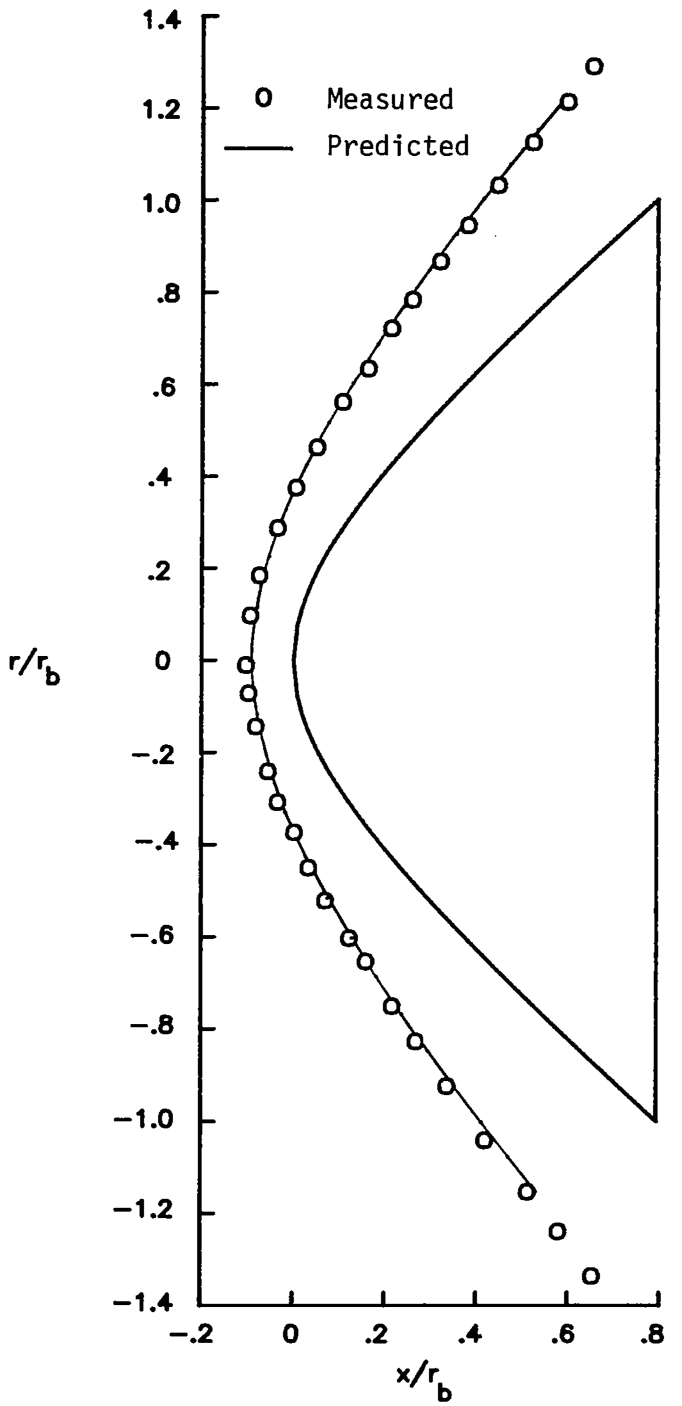

(a) $\alpha = 0°$.

Figure 15.- Measured and predicted shock shapes on the hyperboloid.

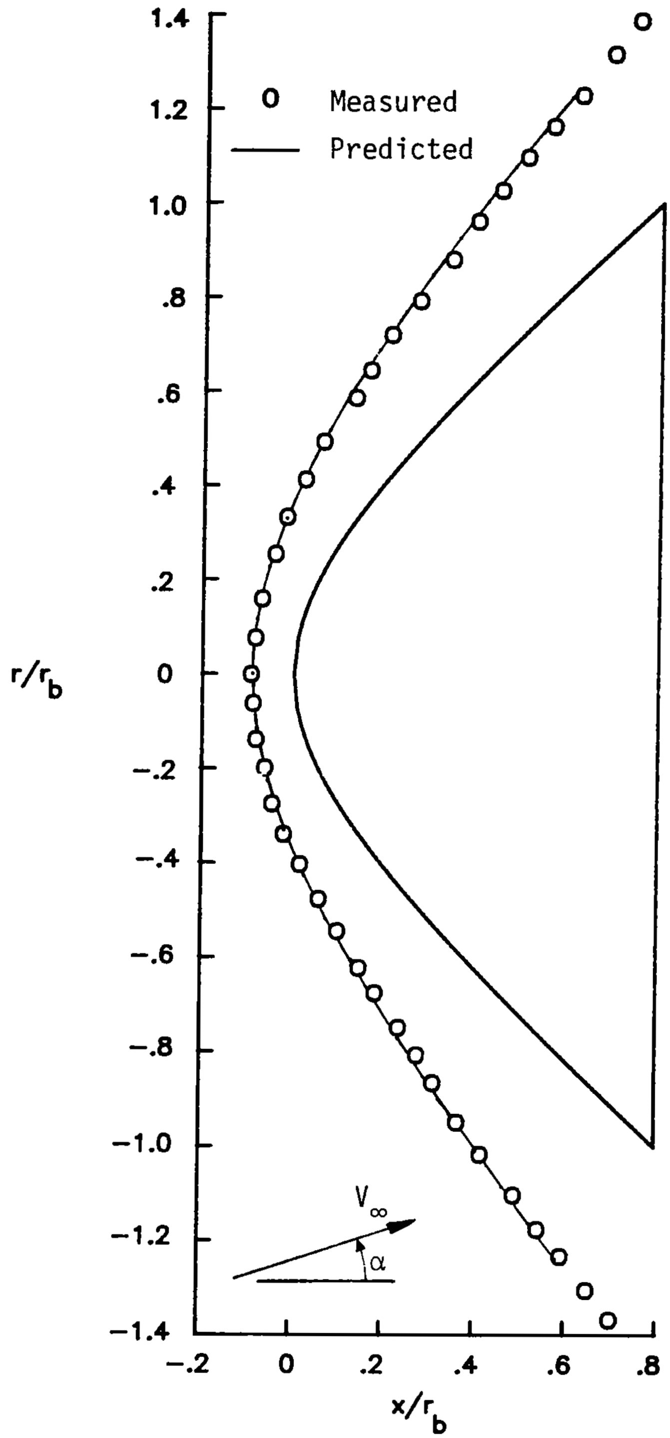

(b) $\alpha = 5°$.

Figure 15.- Continued.

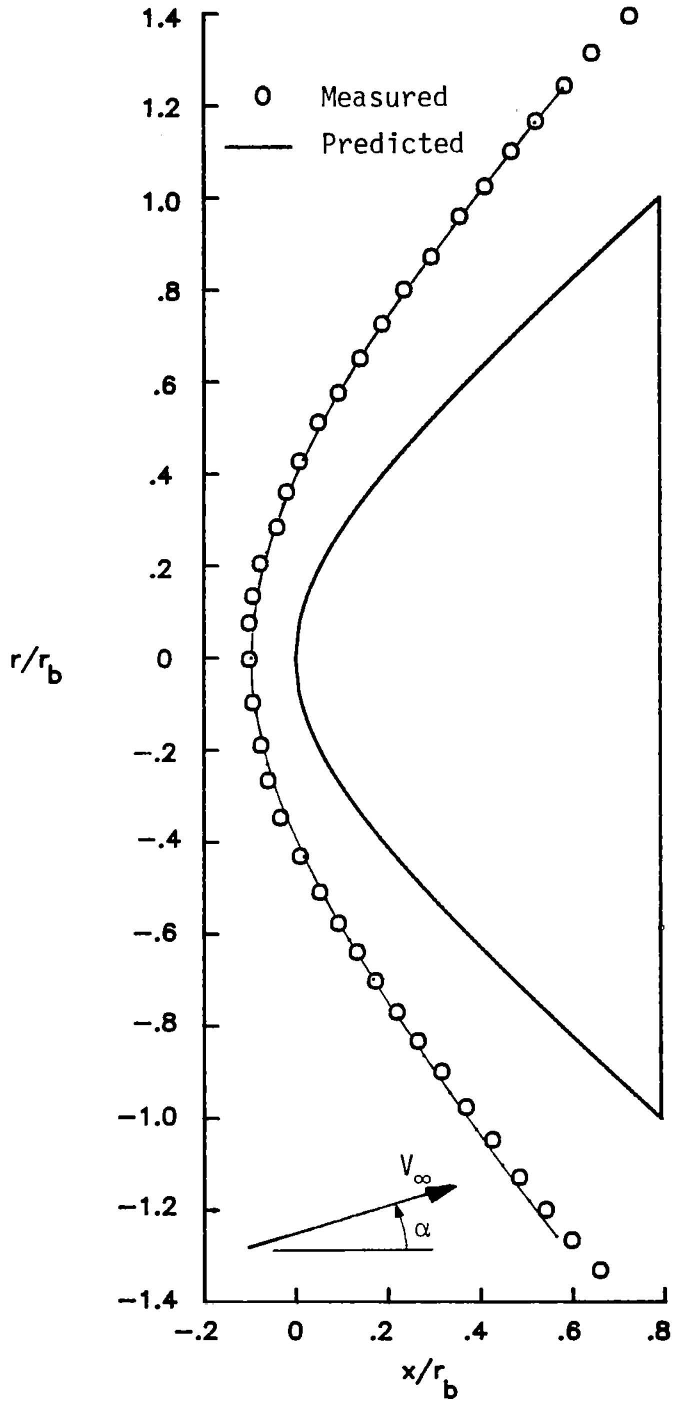

(c) $\alpha = 10°$.

Figure 15.- Continued.

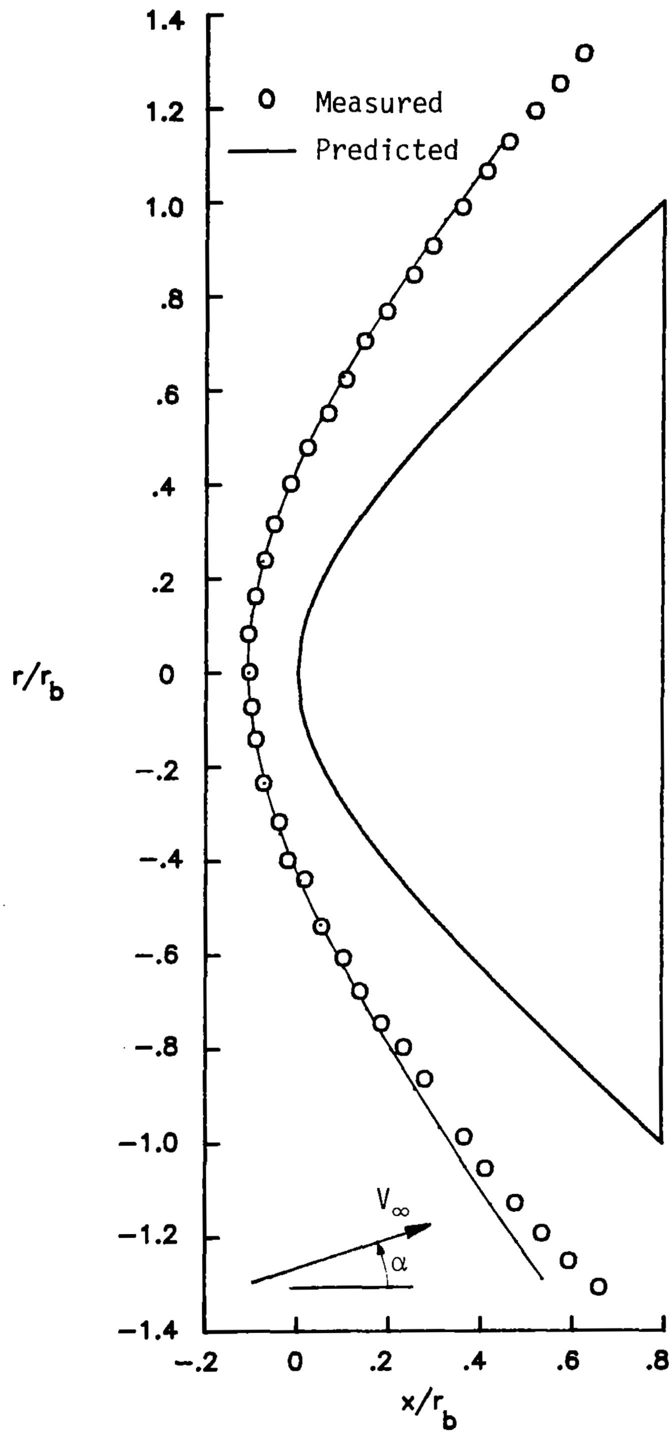

(d) $\alpha = 15°$.

Figure 15.- Concluded.

1. Report No.	2. Government Accession No.	3. Recipient's Catalog No.
NASA TP-2100		

4. Title and Subtitle	5. Report Date
PRESSURES, FORCES AND MOMENTS, AND SHOCK SHAPES FOR A GEOMETRICALLY MATCHED SPHERE-CONE AND HYPERBOLOID AT MACH 20.3 IN HELIUM	January 1983
	6. Performing Organization Code 506-51-13-02
7. Author(s) Robert L. Calloway	8. Performing Organization Report No. L-15499
	10. Work Unit No.
9. Performing Organization Name and Address NASA Langley Research Center Hampton, VA 23665	11. Contract or Grant No.
	13. Type of Report and Period Covered Technical Paper
12. Sponsoring Agency Name and Address National Aeronautics and Space Administration Washington, DC 20546	14. Sponsoring Agency Code

15. Supplementary Notes

16. Abstract

An investigation was conducted to compare measured and predicted pressure distributions, forces and moments, and shock shapes on a geometrically matched sphere-cone and hyperboloid. A hyperboloid with a nose radius of 0.5276 in. and an asymptotic angle of 39.9871° was matched to a sphere-cone with a nose radius of 0.750 in. and a cone half-angle of 45°. Experimental results in helium at a free-stream Mach number of 20.3 and a free-stream unit Reynolds number of 6.83×10^6 per foot were combined with predicted results from a theoretical method to compare the two shapes. Comparisons of experimental results showed small differences in the two shapes, but the prediction method provided better results for the hyperboloid than for the sphere-cone.

17. Key Words (Suggested by Author(s))	18. Distribution Statement
Sphere-cone Hyperboloid Planetary entry	Unclassified - Unlimited Subject Category 34

19. Security Classif. (of this report)	20. Security Classif. (of this page)	21. No. of Pages	22. Price
Unclassified	Unclassified	71	A04

For sale by the National Technical Information Service, Springfield, Virginia 22161

NASA-Langley, 1983